Julius-Maximilians-University of Würzburg

Department of Geography and Geology

Cumulative Habilitation Thesis

Collective Sensing and Artificial Intelligence Techniques for Natural Hazard Risk and Impact Assessment

Prof. Dr. Christian Geiß

Mentors:

Univ.-Prof. Dr. rer. nat. habil. Stefan Dech (Chairman)

Univ.-Prof. Dr. rer. nat. habil. Heiko Paeth

Univ.-Prof. Dr. rer. nat. habil. Hannes Taubenböck

Würzburg, January 2024

„Fragen Sie einen Philosophen, was die Essenz des Menschseins ist, (…). Akademiker sind vielleicht der Meinung, ihre Essenz sei die Fähigkeit, die Welt zu verstehen, über dem Informationsstrom der physischen Sinne zu stehen und die Bedeutung des Wahrgenommenen zu begreifen. Sie evaluieren, beurteilen und treffen Voraussagen. Sie verstehen. Das ist Dopamin."

Daniel Z. Lieberman & Michael E. Long

ACKNOWLEDGEMENTS

I extend my deep gratitude to everyone who contributed to this work.

Additionally, I would like to express my special appreciation to a few individuals:

Prof. Stefan Dech, for providing me with the unique opportunity to pursue a habilitation under his guidance and for anchoring the topic at an institutional level; Prof. Hannes Taubenböck, for his continuous enthusiastic support, sharing of ideas and resources, and his encouraging guidance on approaching problems and situations—especially during challenging times; and Prof. Heiko Paeth, for the invaluable support throughout the process of pursuing a habilitation, for which I am genuinely grateful.

I would like to thank Prof. Günter Strunz for providing the resources and foresight necessary to establish long lines of research.

I was very fortunate that I had the opportunity to work with Patrick Aravena Pelizari. It was always a great feeling working together on methodological problems and overcoming detailed technical obstacles that made the difference at the very end.

I express my gratitude to Dr. Yue Zhu for opening new pathways to anticipate natural hazard risks and for the constant enthusiasm in identifying, addressing, and overcoming problems frequently related to disciplinary boundaries. Special thanks to Dr. Marc Wieland and Dr. Massimiliano Pittore for their inspiring and pioneering works concerning the exploitation of street-level imagery and the consideration of multi-hazard exposure concepts. I also appreciate the insightful exchanges with Prof. Vitor Silva on ways to assess natural hazard risks, with Prof. Emily So on leveraging data from past disasters for anticipation of future events, and with Prof. Thomas Esch on exploring new opportunities to describe natural hazard-prone settlement areas globally.

I would like to thank Dr. Elisabeth Schöpfer and Dr. Torsten Riedlinger for creating and providing unique opportunities to carry out the scientific work outlined in this thesis, and for their alignment with stakeholders and end users.

Additionally, I express my gratitude to the following colleagues for their contributions to the individual works that became part of this cumulative habilitation thesis: Prof. Paula Aguirre, Dr. Ronita Bardhan, Stefan Bauer, Lukas Blickensdörfer, Vanessa Borst, Elisabeth Brzoska, Dr. Tzu-Hsin Karen Chen, Prof. Alexander Fekete, Dr. Juan Camilo Gomez Zapata, Sandro Groth, Dr. Sven Harig, Prof. Masakazu Hashimoto, Prof. Ying Jin, Prof. Shunichi Koshimura, Prof. Samuel Kounev, Marlene Kühnl, Prof. Sven Lautenbach, Dr. Tobias Leichtle, Robert Leppich, Dr. Mariangela Liuzzi, Jana Maier, Prof. Erick Mas, Prof. Antonio Masi, Yvonne Merino Pena, Prof. Lichao Mou, Prof. Luis Moya, Konstantin Müller, Peter Priesmeier, Dr. Chunping Qiu, Alexander Rabuske, Prof. Hernan Santa Maria, Dr. Marta Sapena-Moll, Prof. Andreas Schmitt, Prof. Michael Schmitt, Henrik Schrade, Prof. Stefan Siedentop, Angelica Soto, Ines Standfuß, Prof. Valerio Tramutoli, Ozan Tuncbilek, Mabe Villar-Vega, Dr. Michael Wurm, and Prof. Xiao Xiang Zhu.

I want to thank Prof. Tobias Ullmann and Dr. Martin Wegmann for their support regarding the submission process at the Julius-Maximilians-University of Würzburg.

I am very grateful for the loving support of my father, Ottmar, my sister, Vanessa, and my deceased mother, Marion, who suffered from a very rare disease for which science did not yet have a proper answer.

CONTENTS

LIST OF FIGURES

LIST OF TABLES

LIST OF ABBREVIATIONS

AI	Artificial Intelligence
CNN	Convolutional Neural Networks
CPP	classification post-processing
DL	deep learning
DRCNN	Deep Relearning Convolutional Neural Networks
DSM	digital surface model
DTM	digital terrain model
EO	earth observation
GEM	Global Earthquake Model
HSE	human settlement extent
LSTM	Long Short-Term Memory
LULC	land use and land cover
ML	machine learning
MSER	multistrategy ensemble regression
MTR	multi-task regression
nDSMs	normalized Digital Surface Models
OBV	object-based voting
PSHA	probabilistic seismic hazard assessment
RF	Random Forest
RS	remote sensing
SBST	seismic building structural type
SVM	Support Vector Machines
SVs	support vectors
TDM	spaceborne radar interferometer TanDEM-X
VHR	very high resolution
VSVM	Virtual Support Vector Machines

Synthesis: **Collective Sensing and Artificial Intelligence Techniques for Natural Hazard Risk and Impact Assessment**

1. Introduction

Natural hazards represent a recurring threat to humankind. *Geophysical events* such as earthquakes, tsunamis, and volcanic eruptions, *meteorological events* such as storms, *hydrological events* such as floods and mass movements, as well as *climatological events* such as heat waves, droughts, and forest fires cause an enormous number of fatalities and economics losses. Over the past four decades, documented extensively by entities such as the reinsurance cooperation MunichRe, a notable upward trend is evident in both the frequency of loss events and the corresponding economic losses [1]. Thereby, *hydrological disasters* were the most frequent events, directly followed by *meteorological disasters*. The latter caused the highest monetary losses, whereas *geophysical disasters* were the deadliest events due to a short onset period (time between first occurrence of an event and its peak in intensity). Overall, more than 1.72 million people lost their lives in a natural catastrophe within that time period, which corresponds to more than 120 people per day on average. Simultaneously, more than 4 600 billion US$ of both insured and non-insured economic values were lost [1].

Simultaneously, there has been a global population rise from 4.44 billion individuals in 1980 to over 8 billion by the end of 2022 [2]. This surge is accompanied by a substantial transformation of human habitats, with more individuals residing in urban regions compared to rural ones since 2008. Projections indicate a persistent trend toward urbanization, with an expected two-thirds of the global population projected to inhabit cities by the year 2050. Furthermore, the most recent estimates from the United Nations indicate a potential global population rise to approximately 8.5 billion by 2030, 9.7 billion by 2050, and 10.4 billion by 2100 [2]. As a result, natural hazards that previously had rather little impact, striking sparsely populated areas, now have the potential to affect densely populated urban centers. Moreover, many hazards do not manifest in isolation but rather create intricate sequences of events with cascading effects [3]. Also, the process of urbanization can exacerbate the vulnerability of built environments. The swift expansion of urban areas, particularly occurring in developing nations [4], frequently involves the construction of unplanned and highly vulnerable settlements, where measures to mitigate the impact of natural hazards are often neglected [5].

Despite advancements, the creation of risks is surpassing efforts in risk reduction. Disasters, economic losses, and the root vulnerabilities contributing to risk, such as poverty and inequality, are on the rise. If left unaddressed, this trend is anticipated to result in unprecedented casualties, substantial economic and ecological damages, and a substantial threat to civil security and sustainable development in the future. Effectively mitigating these perils necessitates a comprehensive understanding of the associated risks [5]. Particularly for the estimation of losses induced by natural hazards, gathering detailed information on building inventories and population in hazard-prone areas (i.e., exposure data) is typically the most time-intensive and costly aspect. Traditional methods of information collection, such as in-depth *in-situ* building analyses conducted by structural engineers and small-scale population surveys, are increasingly inadequate in dealing with the rapid spatiotemporal changes in built environments [6].

In response to the need for spatially continuous exposure information over extensive areas, various approaches recognized earth observation (EO) data as a valuable information source. This is particularly evident with the latest generation optical sensors that facilitate a detailed characterization of built environments in areas prone to hazards. Various studies established an integrated perspective on vulnerability, considering numerous parameters for a comprehensive assessment. Consequently, research focused on extracting a diverse range of exposure-related parameters from remote sensing (RS), including properties of the built environment and population characteristics, as explored in studies such as [7]-[13].

Simultaneously, the demands for data, which include requirements for very high spatial resolution EO imagery and detailed *in-situ* data, pose challenges for the application of numerous aforementioned approaches. Issues such as data availability, the monetary costs associated with acquiring data, and the computational demands of processing further hinder the widespread use of these methods. Additionally, local idiosyncrasies must not be bypassed, and the transfer of models cannot be carried out in a non-adaptive manner. For instance, similar building structural types may exhibit considerable variability in morphological appearance and vulnerability across different regions worldwide. Consequently, building inventory information and population data, along with associated vulnerability properties, are often outdated, spatially discontinuous, strongly aggregated, and, in numerous natural hazard-prone regions, completely nonexistent [14]. Consequently, strategies for natural hazard risk assessment often fall short of providing a comprehensive view on risk on large scales while maintaining a high spatial, thematic, and temporal resolution.

Is there any hope? I believe so. Recently, there have been substantial advancements in global-scale data collection mechanisms. State-of-the-art EO missions, such as ESA's Sentinel-2 mission [15] and DLR's spaceborne radar interferometer TanDEM-X (TDM) [16], [17], are gathering planetary data with unprecedented spatial and temporal resolution properties, particularly relevant for characterizing built environments. Furthermore, a diverse array of complementary data sources is emerging to characterize built environments. These sources comprise geospatial vector data compiled by volunteers (e.g., OpenStreetMap [18]), *in-situ* data (e.g., collected with ground-based omnidirectional imaging systems [19] or accessible via platforms such as Google Street View [20]), or data provided in social networks by people sensing the environment (e.g., geo-located Tweets [21]) [3]. In parallel, advanced data processing models evolved from the Machine Learning (ML) domain. The shift from expert-based systems, employing dedicated if-then rules for extracting thematic information, to ML-based methods, that automatically derive rules from empirical observations, is ongoing. Today, sophisticated algorithms related to Artificial Intelligence (AI) [22] enable the efficient and reliable extraction of thematic information from multimodal geospatial data. Consequently, this habilitation aims to substantially support and enable risk and impact assessment procedures by exploring new geospatial data sources and designing novel methods mainly related to the field of ML and AI to extract thematic information with the focus on natural hazard risk-related exposure.

2. Goals

In this habilitation, we propose novel methods related to the fields of ML and AI for beneficial processing of geospatial data. Such methods learn a model from limited but properly encoded prior knowledge to assign a thematic label (e.g., a structural type) to an instance under analysis (e.g., a building) and are particularly useful when an explicit modelling based on, e.g., mechanical models, is too complex. At the same time, such approaches need both a sufficient amount of prior knowledge and viable descriptors characterizing the instances under analysis to achieve a high predictive accuracy. In the past, the compilation of prior knowledge was very costly and dominantly hampered learning and application of models. However, data that allow the compilation of relevant prior knowledge become more ubiquitous. As such, this work uniquely exploits multiple heterogeneous data sources which provide relevant thematic information. These comprise ground-based imagery (e.g., Google Street View) and Volunteered Geographic Information (e.g., OpenStreetMap), among others. For the compilation of descriptors of built environments, we propose innovative techniques to extract information from satellite missions with global coverage in conjunction with a high spatial resolution (including Landsat, Sentinel-2, TDM). Thus, from a *data-oriented perspective*, the habilitation aims for addressing the task:

- How can multisource geospatial data be harvested and deployed for natural hazard-related exposure mapping with a high degree of automatization? (goal 1)

To derive thematic information from the multisource data with viable accuracies, we propose novel ML and AI-based workflows which infer the prior knowledge in a beneficial way. The goal is to learn models that are able to allow for high predictive performance and transferability. The latter also comprises the particular implementation of domain adaptation capabilities. Thereby, invariant models are learned on a specific geographic region. However, they also enable viable predictions for other geographic regions, where less or no prior knowledge is available. At the same time, we are interested in so-called multitask learning approaches. Such models are not strictly optimized for a single target variable. Instead, the goal is to learn an efficient solution w.r.t. multiple target variables simultaneously. The compilation of exposure information in a multi-hazard context allows capitalizing upon synergy effects, since multiple exposure components must be assigned to an instance under analysis and those components are frequently relevant w.r.t. multiple hazards (e.g., the assignment of structural type, occupancy, and roof type to a building). From a *methods-oriented information extraction perspective*, the habilitation aims for contributing to the question:

- How must ML/AI-based models be designed to enable the extraction of exposure and damage information with state-of-the-art generalization capabilities? (goal 2)

The described combination of data and techniques aligns with a collective sensing approach. Such an approach recognizes that relying on a solitary data source is frequently inadequate for meeting the information requirements necessary to analyze intricate built environments undergoing changes across various spatial and temporal dimensions. Given the joint exploitation of multiple data sources, the habilitation aims to satisfy the information needs required to map, monitor, and ultimately understand and manage built environments w.r.t. risks in hazard-prone regions. Thus, *from an epistemological-oriented view* on natural hazard risk, the habilitation addresses the question:

- To what extent are cities and societies nowadays and in the future threatened and affected by natural hazards? (goal 3)

This knowledge is strongly required to anticipate probable future damage, to inform local populations and authorities about their current level of risk, as well as to implement appropriate mitigation measures.

3. Publications

The publications relevant for the habilitation are listed in Tab. 3-1 and provided in Appendix A. For this cumulative habilitation thesis (according to §7.3.2 of the habilitation regulations), ten peer-reviewed journal papers as first author and ten peer-reviewed journal papers as co-author are provided in accordance with the mentoring agreement, dated March 11th, 2020. The listed articles were published in international journals between 2019 and 2023 and have all undergone a peer review process by at least two reviewers. The work was carried out in cooperation with various national and international working groups and mostly in the context of ongoing research projects. Fig. 3-1 groups the papers schematically according to their focus w.r.t. to exploring and generating new data (sources), proposing novel methods, and enabling innovative applications in the field of natural hazard risk and impact assessment. In addition, Tab. 3-2 shows the objectives of the individual papers and assigns their contributions to the overarching objectives of the habilitation mentioned in section 2.

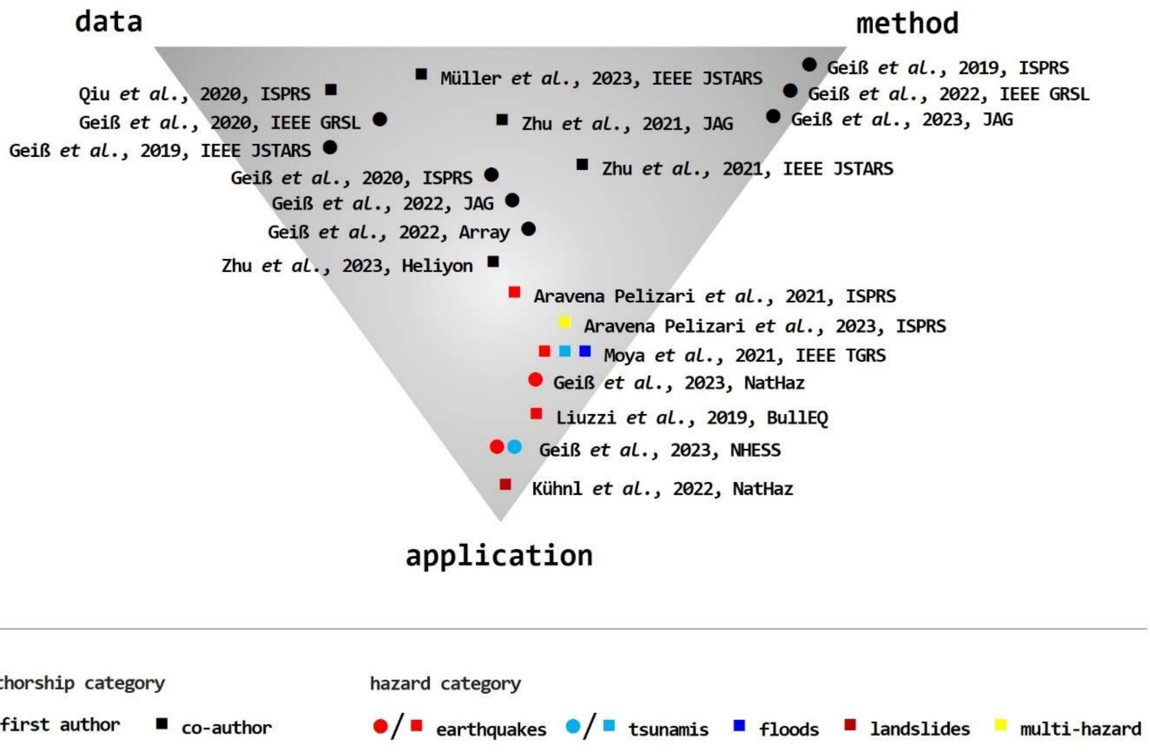

Fig. 3-1. Qualitative categorization of the papers according to their focus w.r.t. to exploring and generating new *data* (sources), proposing novel *method*s, and enabling innovative *application*s in the field of natural hazard risk and impact assessment. The considered natural hazard(s) for the rather *application*-oriented works are also indicated.

TAB. 3-1. OVERVIEW OF PEER-REVIEWED AND HABILITATION-RELEVANT PUBLICATIONS AS (a) FIRST AUTHOR AND (b) CO-AUTHOR

(a)
C. Geiß, P. Aravena Pelizari, L. Blickensdörfer, and H. Taubenböck, "Virtual Support Vector Machines with Self-Learning Strategy for Classification of Multispectral Remote Sensing Imagery," *ISPRS Journal of Photogrammetry and Remote Sensing*, vol. 151, pp. 42–58, 2019.
C. Geiß, P. Aravena Pelizari, O. Tuncbilek, and H. Taubenböck, "Semi-supervised Learning with Constrained Virtual Support Vector Machines for Classification of Remote Sensing Image Data," *International Journal of Applied Earth Observation and Geoinformation*, vol. 125, 103571, 2023.
C. Geiß, Y. Zhu, C. Qiu, L. Mou, X. X. Zhu, and H. Taubenböck, "Deep Relearning in the Geospatial Domain for Semantic Remote Sensing Image Segmentation," *IEEE Geoscience and Remote Sensing* Letters, vol. 19, 8002705, 2022.
C. Geiß, P. Aravena Pelizari, S. Bauer, A. Schmitt, and H. Taubenböck, "Automatic Training Set Compilation with Multisource Geodata for DTM Generation from the TanDEM-X DSM," *IEEE Geoscience and Remote Sensing Letters*, vol. 17, no. 3, pp. 456–460, 2022.
C. Geiß, T. Leichtle, M. Wurm, P. Aravena Pelizari, I. Standfuß, X. X. Zhu, E. So, S. Siedentop, T. Esch, and H. Taubenböck, "Large-Area Characterization of Urban Morphology – Mapping Built-Up Height and Density with the TanDEM-X Mission and Sentinel-2," *IEEE Journal of Selected Topics in Applied Earth Observation and Remote Sensing*, vol. 12, no. 8, pp. 2912–2927, 2019.
C. Geiß, H. Schrade, P. Aravena Pelizari, and H. Taubenböck, "Multistrategy Ensemble Regression for Mapping of Built-Up Height and Density with Sentinel-2 Data," *ISPRS Journal of Photogrammetry and Remote Sensing*, vol. 170, pp. 57–71, 2020.
C. Geiß, E. Brzoska, P. Aravena Pelizari, S. Lautenbach, and H. Taubenböck, "Multi-target Regressor Chains with Repetitive Permutation Scheme for Characterization of Built Environments with Remote Sensing," *International Journal of Applied Earth Observation and Geoinformation*, vol. 106, 102657, 2022.
C. Geiß, A. Rabuske, P. Aravena Pelizari, S. Bauer, and H. Taubenböck, "Selection of Unlabeled Source Domains for Domain Adaptation in Remote Sensing," *Array*, vol. 15, 100233, 2022.
C. Geiß, P. Priesmeier, P. Aravena Pelizari, A. Soto, E. Schöpfer, T. Riedlinger, M. Villar Vega, H. Santa Maria, C. Gomez Zapata, M. Pittore, E. So, A. Fekete, and H. Taubenböck, "Benefits of Global Earth Observation Missions for Disaggregation of Exposure Data and Earthquake Loss Modelling – Evidence from Santiago de Chile," *Natural Hazards*, vol. 119, pp. 779–804, 2023.
C. Geiß, J. Maier, E. So, E. Schoepfer, S. Harig, J. C. Gómez Zapata, and Y. Zhu, "Anticipating a risky future: LSTM models for spatiotemporal extrapolation of population data in areas prone to earthquakes and tsunamis in Lima, Peru," *Natural Hazards and Earth System Sciences*, forthcoming, 2023. https://doi.org/10.5194/egusphere-2023-1794

(b)
C. Qiu, M. Schmitt, **C. Geiß**, T-H. K. Chen, and X. X. Zhu, "A framework for large-scale mapping of human settlement extent from Sentinel-2 images via fully convolutional networks," *ISPRS Journal of Photogrammetry and Remote Sensing*, vol. 163, pp. 152–170, 2020.
K. Müller, R. Leppich, **C. Geiß**, V. Borst, P. Aravena Pelizari, S. Kounev, and H. Taubenböck, "Deep Neural Network Regression for Digital Surface Model Generation with Sentinel-2 Imagery," *IEEE Journal of Selected Topics in Applied Earth Observation and Remote Sensing*, vol. 16, pp. 8508–8519, 2023.
P. Aravena Pelizari, **C. Geiß**, P. Aguirre, H. Santa María, Y. Merino Peña, and H. Taubenböck, "Automated building characterization for seismic risk assessment using street-level imagery and deep learning," *ISPRS Journal of Photogrammetry and Remote Sensing*, vol. 180, pp. 370–386, 2021.
P. Aravena Pelizari, **C. Geiß**, S. Groth, and H. Taubenböck, "Deep multitask learning with label interdependency distillation for multicriteria street-level image classification," *ISPRS Journal of Photogrammetry and Remote Sensing*, vol. 204, pp. 275–290, 2023.
M. Liuzzi, P. Aravena Pelizari, **C. Geiß**, A. Masi, V. Tramutoli, and H. Taubenböck, "A Transferable Remote Sensing Approach to Classify Building Structural Types for Seismic Risk Analyses: the case of Val d'Agri Area (Italy)," *Bulletin of Earthquake Engineering*, vol. 17, pp. 4825–4853, 2019.
M. Kühnl, M. Sapena, M. Wurm, **C. Geiß**, and H. Taubenböck, "Multitemporal Landslide Exposure and Vulnerability Assessment in Medellín, Colombia," *Natural Hazards*, vol. 119, pp. 883–906, 2022.
L. Moya, **C. Geiß**, M. Hashimoto, E. Mas, S. Koshimura, and G. Strunz, "Hazard Intensity-Based Selection of Training Samples for Remote Sensing Building Damage Classification," *IEEE Transactions on Geoscience and Remote Sensing*, vol. 59, no. 10, pp. 8288–8304, 2021.
Y. Zhu, **C. Geiß**, and E. So, "Image Super-Resolution with Dense-sampling Residual Channel-Spatial Attention Networks for Multi-temporal Remote Sensing Image Classification," *International Journal of Applied Earth Observation and Geoinformation*, vol. 104, 102543, 2021.
Y. Zhu, **C. Geiß**, E. So, and Y. Jin, "Multi-temporal Relearning with Convolutional LSTM Models for Land Use Classification," *IEEE Journal of Selected Topics in Applied Earth Observation and Remote Sensing*, vol. 14, pp. 3251–3265, 2021.
Y. Zhu, **C. Geiß**, E. So., R. Bardhan, H. Taubenböck, and Y. Jin, "Urban expansion simulation with an explainable ensemble deep learning framework," *Heliyon*, forthcoming, 2023.

TAB. 3-2. PUBLICATIONS, OBJECTIVES, AND CONTRIBUTION TO GOALS

publication	objectives and contribution to the goals of the habilitation	
Section 4: Novel AI-based algorithms for the interpretation of RS imagery		
Geiß *et al.*, 2019, ISPRS	We establish a self-learning procedure to ultimately prune non-informative virtual samples from a possibly arbitrary invariance generation process to allow for robust and sparse model solutions in the context of Virtual Support Vector Machines (VSVM) for RS image classification.	goal 2
Geiß *et al.*, 2023, JAG	We introduce two semi-supervised models for the classification of RS image data. The models are built upon the framework of VSVM and are particularly useful in situations with a very limited amount of available prior knowledge, i.e., labeled samples.	goal 2
Geiß *et al.*, 2022, IEEE GRSL	We present a classification post-processing (CPP) technique based on Fully Convolutional Neural Networks (CNN) for semantic RS image segmentation.	goal 2
Section 5: Novel techniques for the characterization of the built environment with EO data		
Qiu *et al.*, 2020, ISPRS	We present a deep-learning-based framework to automatically map human settlement extent (HSE) from multi-spectral Sentinel-2 data using regionally available geo-products as training labels.	goal 1
Müller *et al.*, 2023, IEEE JSTARS	We explore to extract high-resolution normalized Digital Surface Models (nDSMs) from low resolution Sentinel-2 data by using U-Net as a base architecture while integrating tailored multiscale encoders with differently sized kernels in the convolution as well as conformed self-attention inside the skip connection gates.	goal 1, goal 2
Geiß *et al.*, 2020, IEEE GRSL	We propose an automatic workflow for digital terrain model (DTM) generation from TDM digital surface model (DSM) data through additional consideration of Sentinel-2 imagery and open-source geospatial vector data.	goal 1, goal 2
Geiß *et al.*, 2019, IEEE JSTARS	We establish a novel multistep procedure for morphologic characterization of built environments in terms of built-up density and built-up height. Thereby, we rely on elevation measurements from the TDM and multispectral Sentinel-2 imagery.	goal 1, goal 2
Geiß *et al.*, 2020, ISPRS	We establish a workflow for estimation of built-up density and built-up height based on multispectral Sentinel-2 data while introducing a novel ensemble regression approach.	goal 1, goal 2
Geiß *et al.*, 2022, JAG	We propose a novel multi-task learning technique by implementing Multi-target Regressor Chains with repetitive permutation to estimate built-up density and built-up height.	goal 1, goal 2
Geiß *et al.*, 2022, Array	We propose unsupervised source selection by voting from (an ensemble of) similarity metrics that follow aligned marginal distributions regarding image features of source and target domains to select a single source domain for domain adaptation from multiple potentially helpful but unlabeled source domains.	goal 2, goal 1
Section 6: Exposure modelling for natural hazard risk assessment		
Geiß *et al.*, 2023, NatHaz	We exploit measurements from TDM and Sentinel-2 to characterize the built environment to constrain existing exposure data in a spatial disaggregation approach. Further, we estimate losses due to seismic ground shaking and corresponding sensitivity as a function of the resolution properties of the exposure data used in the model.	goal 3, goal 2
Aravena Pelizari *et al.*, 2021, ISPRS	We evaluate the collection of vulnerability-related structural building characteristics based on deep CNNs and street-level imagery such as provided by Google Street View.	goal 1, goal 2, goal3
Aravena Pelizari *et al.*, 2023, ISPRS	We introduce a novel deep multitask learning architecture that specifically encodes cross-task interdependencies within the setting of multiple image classification problems for multi-criteria building characterization using street-level imagery related to risk assessments toward multiple natural hazards.	goal 2, goal 3
Liuzzi *et al.*, 2019, BullEQ	We propose a methodology based on ML algorithms for rapid and robust classification of building structural types in multispectral RS imagery aiming to assess buildings' seismic vulnerability. We show that few geometry features enable generalization capabilities similar to models learned with a large number of features.	goal 3, goal 2
Kühnl *et al.*, 2022, NatHaz	We use heterogeneous input data from RS, landslide hazard maps, and census data to examine how landslide risks evolved over a 24-year period from 1994 to 2018.	goal 3

Section 7: Post-event damage assessment		
Moya *et al.*, 2021, IEEE TGRS	We study disaster events in which the intensity can be modeled via numerical simulation and/or instrumentation. For such cases, two fully automatic procedures for the detection of severely damaged buildings are introduced in the context of post-event damage assessment based on RS.	goal 2, goal 3
Section 8: Anticipating a risky future		
Zhu *et al.*, 2021, JAG	We propose a novel CNN-based framework to enhance the spatial resolution of time series multispectral RS images.	goal 1, goal 2
Zhu *et al.*, 2021, IEEE JSTARS	We present a novel hybrid framework, which integrates spatial–temporal semantic segmentation with postclassification relearning, for multitemporal land use and land cover (LULC) classification based on very high resolution (VHR) satellite imagery.	goal 2, goal 1
Zhu *et al.*, 2023, Heliyon	We present a novel deep learning-based (DL) ensemble framework for urban expansion simulation at an intra-urban granular level.	goal 1, goal 3
Geiß *et al.*, 2023, NHESS	We anticipate geospatial population distributions to quantify the future number of people living in earthquake-prone and tsunami-prone areas of Lima and Callao, Peru, using ML models tailored for time series analysis, i.e., Long Short-Term Memory-based (LSTM) networks.	goal 3, goal 2

4. Novel AI-based algorithms for the interpretation of RS imagery

The development of methods for extracting information from RS imagery has been one of the major tasks of the scientific RS community in recent years. In this context, various strategies were employed to derive thematic information from image data. Two primary approaches include expert-based systems and statistical learning methods. Expert-based systems involve a set of if-then rules devised by one or more experts. On the other hand, statistical learning methods encompass techniques that establish rules based on empirical observations, utilizing labeled samples. Within statistical learning techniques, supervised methods stand out as one of the most popular groups of classification approaches, known for their robust and accurate information extraction capabilities. The core concept of these approaches is to deduce a decision rule (e.g., a function) from limited but properly encoded prior knowledge, i.e., labeled training samples. This enables the accurate assignment of class labels for unseen (i.e., unlabeled) samples.

4.1 Geiß *et al.*, 2019, ISPRS: VSVM with self-learning for classification of RS imagery

In addressing classification problems that involve (i) a limited number of labeled training samples, (ii) a high number of features, and (iii) complex, nonlinear class distributions, several non-parametric ML algorithms emerged as viable options. Their algorithmic characteristics make them particularly relevant for such scenarios. Support Vector Machines (SVM) stand out as an approach in this application context, offering effective handling of complex RS classification problems [23]. SVM operate based on the principle of structural risk minimization, suggesting a tradeoff between the accuracy of an approximation and the complexity of the associated approximation function. SVM identify an appropriate set of parameters to fit a decision surface, i.e., the hyperplane, between different classes of labeled samples. To handle nonlinear problems, the labeled samples undergo a nonlinear transformation $\phi(\cdot)$ from the input space into a higher-dimensional space. In this transformed space, the optimal separating hyperplane maximizes the margin between patterns of different classes and the hyperplane. The maximized margin is described by two additional marginal hyperplanes that border the samples closest to the separating surface, referred to as support vectors (SVs) [24]. This unique property allows the definition of the model based only on these SVs, enabling the construction of robust models with high generalization capabilities from a relatively small number of labeled training samples. Simultaneously, this characteristic of SVM opens the opportunity to efficiently incorporate additional prior knowledge into the classifier. When learning a classification model from labeled samples, it is preferable that the solution is robust to changes in the representation of objects in the data. Such changes may occur due to transformations, such as perturbations and variations in size, alignment, or noise level of the associated signal [25]. The integration of these properties into the classification model, represented by decision functions, renders the algorithm "invariant" [26].

We adopt the concept of learning invariant decision functions for RS image classification using SVM (Fig. 4-1a,b). In this approach, we generate artificially transformed samples, referred to as virtual samples, based on available prior knowledge. Initially, we identify labeled samples closest to the separating hyperplane with the maximum margin—the SVs—by training an initial SVM model. Using the SVs, we create virtual samples by perturbing the features to which the model should exhibit invariance (Fig. 4-1c). Next, we relearn the model using both the SVs and the virtual samples, aiming to modify the hyperplane with the maximum margin and enhance the generalization capabilities of decision functions (Fig. 4-1d). Unlike existing approaches, we introduce a self-learning procedure to prune non-informative virtual samples from a potentially arbitrary invariance generation process. This strategy ensures robust and sparse model solutions. The self-learning process incorporates a joint consideration of a similarity constraint (Fig. 4-1e) and a margin sampling constraint (Fig. 4-1f) before relearning the model to establish a final solution (Fig. 4-1g).

We present an innovative exploration of the invariance generation process within the framework of object-based image analysis. This involves aggregating image elements (pixels) into image objects, represented by segments/superpixels, using a segmentation algorithm. Starting from an initial singular segmentation level, we introduce invariances by adjusting hyperparameters of the segmentation algorithm, focusing on variations in scale and shape.

Our experimental findings are based on two very high spatial resolution multispectral data sets acquired over the city of Cologne, Germany, and the Hagadera Refugee Camp, Kenya. Comparative evaluations of model accuracy underscore the favorable performance properties of the proposed methods, particularly in scenarios with very few labeled samples.

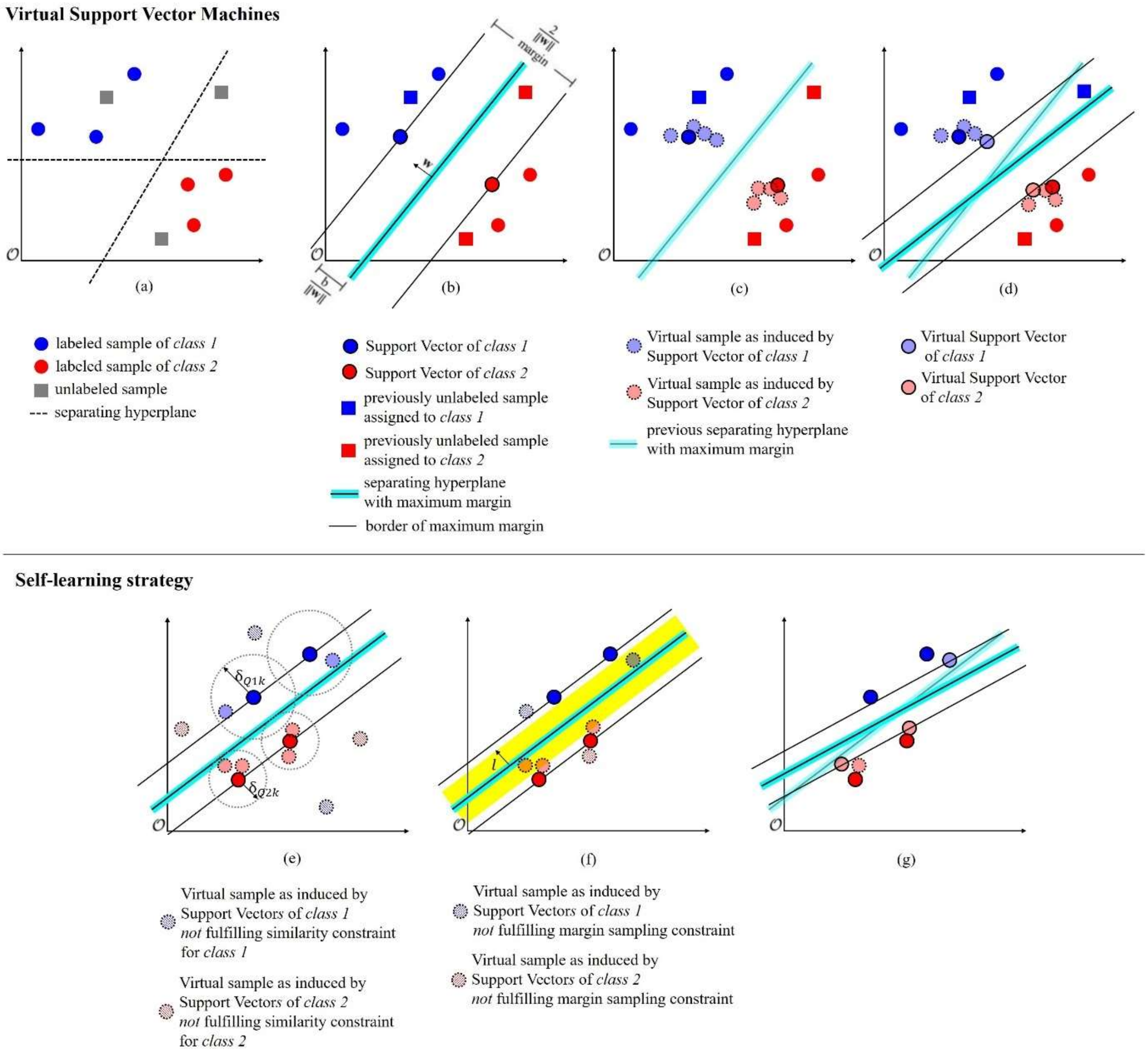

Fig. 4-1. Functionality of VSVM and self-learning. (a) The visualization starts from an arbitrary set of separating hyperplanes that linearly separate the classes of the training samples. (b) Initially, a hyperplane is established that separates the training samples with the maximum margin. Solely labeled samples closest to the separating hyperplane with the maximum margin—the SVs—are required to define the model. (c) SVs are used to generate artificially transformed samples, i.e., virtual samples, to encode invariances. The model is relearned using the labeled samples that became SVs after an initial model run, in conjunction with affiliated virtual samples. This process aims to alter the hyperplane with the maximum margin. Previously unlabeled samples are relabeled according to their position w.r.t. the final separating hyperplane with the maximum margin. (e) Virtual samples are evaluated based on their Euclidean distance to the associated SVs and are pruned from the set of training samples if they exceed an empirically determined class-specific distance. (f) Residual virtual samples are evaluated based on their position to the margin and are pruned from the set of training samples if they exceed a predefined distance. (g) The model is relearned using SVs and residual virtual samples to eventually alter the hyperplane with the maximum margin. We extracted the content of the figure and caption from [27].

4.2 Geiß *et al.*, 2023, JAG: Semi-supervised VSVM for classification of RS imagery

With the previous work we showed that the performance of SVM models can be substantially increased without adding further true prior knowledge. This motivated us to extend the proposed algorithms in the context of semi-supervised learning. Semi-supervised learning frameworks were shown to be particularly useful to allow for robust generalization capabilities in settings with little prior knowledge. Semi-supervised methods aim to encode the structural information related to the unlabeled samples for a better representation of the thematic classes and fitting decision boundaries with a better generalization capability as compared to the deployment of labeled samples alone. In a typical semi-supervised learning procedure, unlabeled samples are iteratively labeled to create semi-labeled samples using an initially learned model. Subsequently, the semi-labeled samples are deployed in conjunction with the labeled ones for learning a final supervised model (Fig. 4-2).

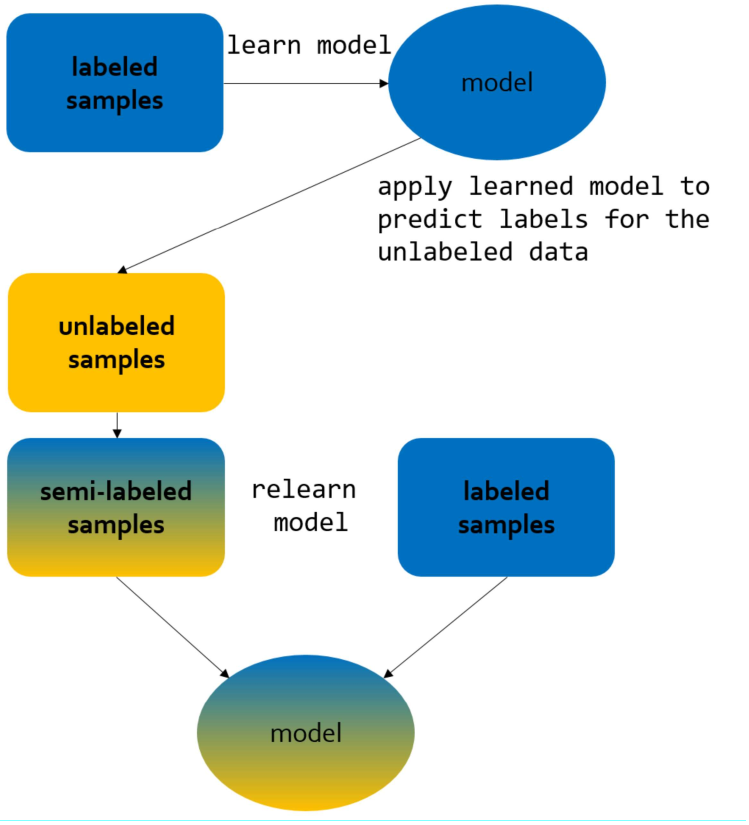

Fig. 4-2. Semi-supervised learning scheme where unlabeled samples are iteratively labeled to create semi-labeled samples using an initially learned supervised model. Subsequently, the semi-labeled samples are deployed in conjunction with the labeled ones for learning a final supervised model.

Nevertheless, inadequately constrained semi-labeled samples have the potential to cause model divergence [28]. Consequently, query functions within active learning and semi-supervised models frequently incorporate opposite criteria. Active learning is centered on identifying the most uncertain unlabeled instances situated closest to decision boundaries, deeming subsequent labeling as reliable [29], [30]. Conversely, query functions in semi-supervised learning emphasize the selection of the most dependable semi-labeled samples, typically those situated farthest from the decision boundary [31]. In this context, the previously proposed VSVM framework, featuring a self-learning strategy, presents a distinctive opportunity to employ a collection of restricted semi-labeled samples for encoding invariances. This framework enables the targeted enhancement of samples utilized in model learning by selectively opting for semi-labeled samples that mirror existing SVs and fulfill margin similarity criteria concerning prior decision boundaries. Our objective in this study is to enhance the generalization capabilities of VSVM models by integrating a set of constrained semi-labeled samples. Consequently, the pool of samples used for model learning is enriched with informative semi-labeled samples, thereby naturally extending the VSVM framework within the realm of semi-supervised learning.

In data scenarios where the geometric resolution is considerably smaller than the objects requiring extraction, the discussed concepts find relevance. This relationship is applicable across various classification challenges, with particular applicability to image data from RS sensors featuring a sub-meter geometric resolution, such as WorldView-I–IV or Pléiades. Additionally, the proposed techniques, which include the generation of invariances, hold significance in RS imagery characterized by limited spectral resolution, as seen in multispectral imagery. This becomes crucial when there is a necessity to derive discriminative information amid high intra-class variability and low inter-class variability. To enhance the VSVM framework, we introduce two innovative algorithms. These algorithms integrate constrained semi-labeled samples and virtual semi-labeled samples, contributing to the encoding of invariances throughout the learning process:

- model 1: the first model expands VSVM by introducing a set of constrained semi-labeled samples to define decision boundaries (Fig. 4-3a-c). Its relevance is demonstrated by classification of multispectral RS imagery characterized by a very high geometric resolution.
- model 2: building on the foundation of the first model, our second model utilizes semi-labeled samples to create semi-labeled virtual samples. Specifically, we modify the image features of semi-labeled samples that transform into semi-labeled SVs after the initial model iterations. Constrained semi-labeled virtual samples are further incorporated in the establishment of the final model (Fig. 4-3d-f).

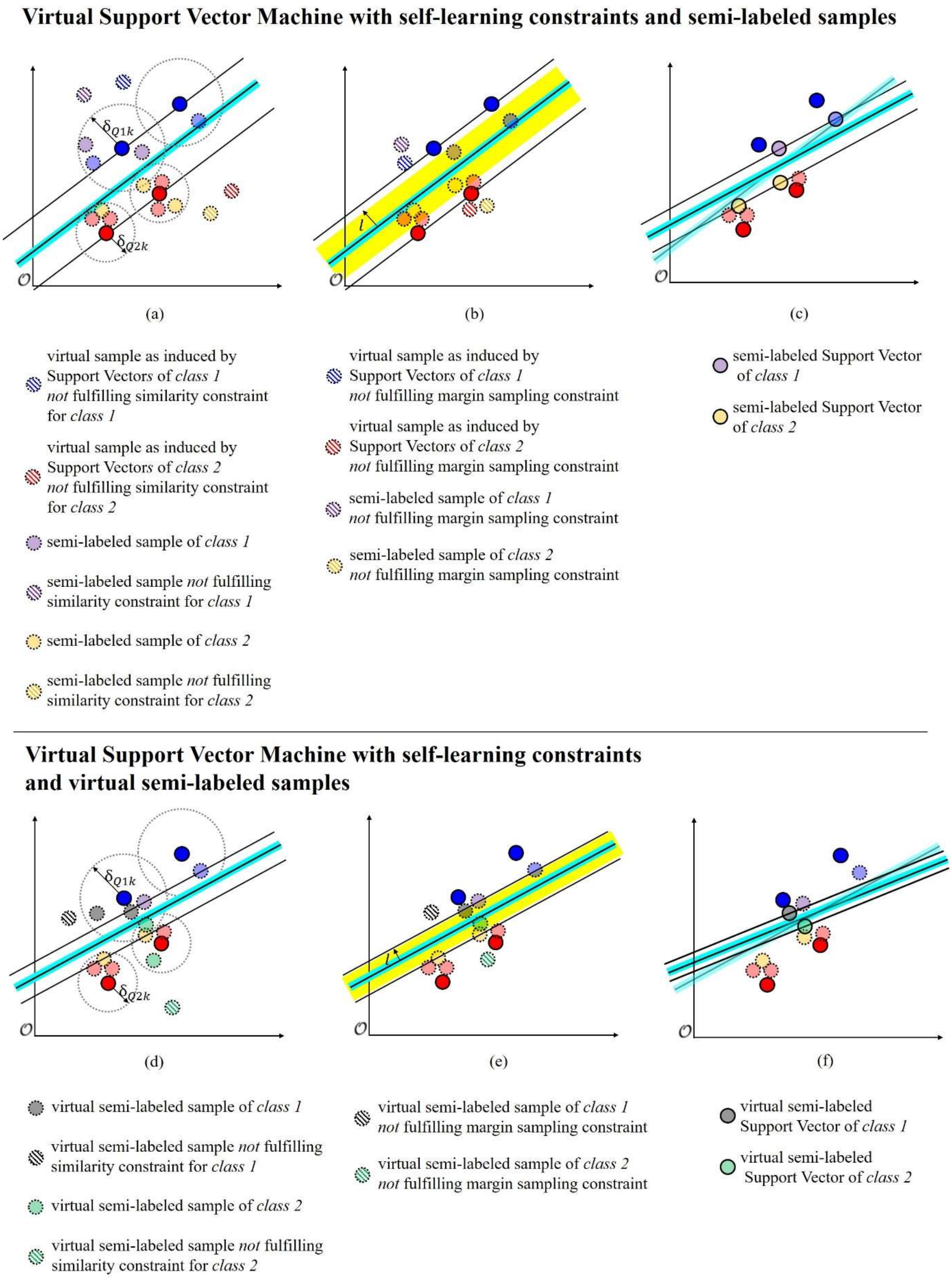

Fig. 4-3. Semi-supervised learning involves self-learning with pruning of both virtual samples and semi-labeled samples from the model. (a) The process includes employing the similarity constraint and (b) the margin sampling constraint to prune virtual and semi-labeled samples before (c) relearning the model. In an extended framework, virtual semi-labeled samples are pruned from the model with (d) the similarity constraint and (e) the margin sampling constraint before (f) relearning the model. We extracted the content of the figure and caption from [32].

The enhanced value of the new semi-supervised VSVM-based models is showcased through benchmarking them against several relevant benchmark models. SVM-single-level: an SVM model is constructed using features derived from the initial segmentation level, i.e., the one model deployed for generating SVs. SVM-multi-level: an SVM is trained using features computed from multiple segmentations. Additional encoded object attributes are represented as extra features, differing from the virtual samples approach employed in the VSVM (a similar method is described in [33]). VSVM-SL (with self-learning constraints): accuracies of the VSVM established with self-learning constraints are integrated. VSVM (without self-learning constraints): the VSVM model without self-learning constraints is also included for comparison. SVM-semi-labeled-SL: a semi-supervised SVM is implemented, adopting a self-learning strategy to incorporate only relevant semi-labeled samples. In addition to these benchmarks, results from both supervised CNNs and semi-supervised CNNs (CNN-semi-labeled) are presented. The two newly proposed models are termed VSVM-SL-semi-labeled and VSVM-SL-virtual-semi-labeled.

Fig. 4-4 illustrates overall accuracies as a function of the number of labeled samples. Both types of invariances demonstrate comparable accuracies in Fig. 4-4a and 4-4b (binary classification problem). The two proposed semi-supervised VSVM models consistently achieve the highest accuracies across the entire range of available prior knowledge and establish a plateau-like performance pattern even with a few labeled samples. A notable competitor is the constrained semi-supervised SVM model (SVM-semi-labeled-SL), which exhibits slightly decreased performance properties, emphasizing the general utility of informative semi-labeled samples. The VSVM-SL approach also attains high accuracy levels, particularly with a limited number of labeled samples, emphasizing the importance of including constrained, informative semi-labeled or virtual samples to prevent model divergence. In contrast, the accuracies of unconstrained VSVM, SVM-single-level, and SVM-multi-level show a performance gap compared to the aforementioned approaches in settings with a few labeled samples. Both CNN-based approaches require a larger number of labeled samples to accelerate accuracy gain and reach a competitive level. The CNN-semi-labeled model provides slight but consistent advantages in accuracy compared to the CNN model.

A similar accuracy pattern is evident in the multiclass classification problem with shape invariance, as shown in Fig. 4-4d. The semi-supervised methods consistently achieve the highest accuracies. The strategy of encoding additional object characteristics as features, rather than virtual samples (SVM-multi-level), results in increasing accuracies only with a growing number of labeled samples, indicating a decrease in overfitting. Along the spectrum of available prior knowledge, the SVM-single-level models are overtaken by the SVM-multi-level models in an ideal-typical manner. This suggests that approaches based on virtual samples avoid issues related to the curse of dimensionality, as no additional dimensions are added to the feature space, which can be disadvantageous in small sample settings. In the case of encoding scale invariance (Fig. 4-4c), the two newly proposed semi-supervised VSVM models frequently exhibit the highest and consistently increasing accuracies. This underscores the advantageous performance properties induced by a constrained set of semi-labeled and virtual semi-labeled samples for model generation.

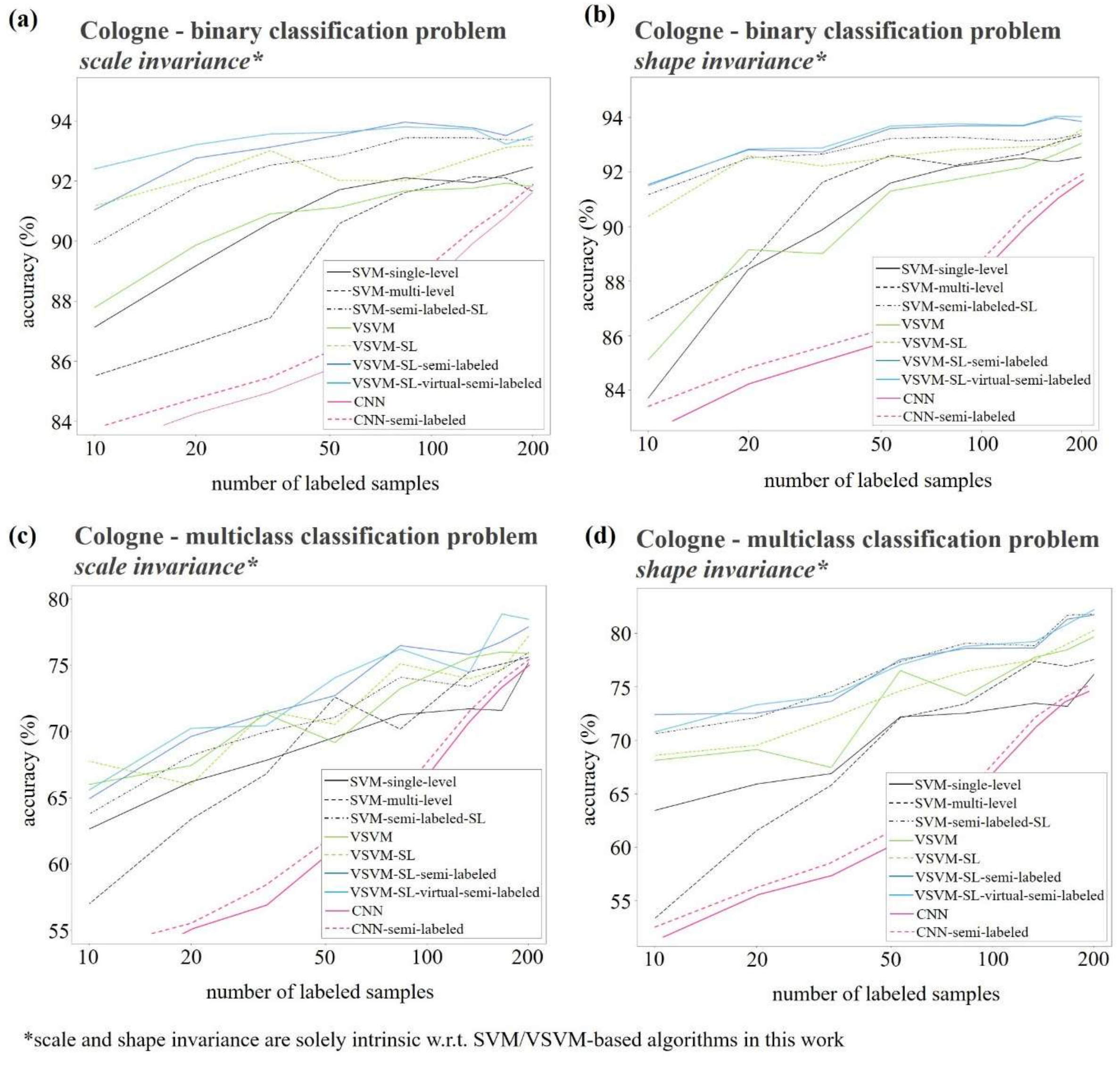

Fig. 4-4. Overall accuracy (% on the y-axis) as a function of the number of labeled samples per thematic class (on the x-axis) for various scenarios: (a) binary classification problem with encoded scale invariance, (b) binary classification problem with encoded shape invariance, (c) multiclass classification problem with encoded scale invariance, and (d) multiclass classification problem with encoded shape invariance. We extracted the content of the figure and caption from [32].

4.3 Geiß *et al.*, 2022, IEEE GRSL: Deep relearning for semantic segmentation

In recent years, DL methods experienced a surge in popularity [34]. The inherent structure of these models often demonstrates strong generalization capabilities, particularly when a substantial amount of prior knowledge is accessible. Models such as fully CNNs [35] excel in learning hierarchical discriminative feature representations, leading to enhanced accuracy in tasks such as pixel-level predictions, i.e., semantic segmentation, when abundant training data is at hand. However, in certain domains, gathering the necessary prior knowledge for DL-based methods can still be an expensive and resource-intensive process.

The refinement of classification outcomes through CPP presents an avenue to potentially improve classification accuracy without introducing additional prior knowledge into the model [36]. In the realm of CPP techniques, most approaches focus on enhancing the initial classification result by leveraging the spatial occurrence and alignment of class labels. Subsequently, these approaches often involve relabeling in the image domain, using methods such as majority filtering [37]. However, recent developments suggest that the concept of relearning can be a more accurate CPP strategy [38]-[40]. In this approach, a supervised classification model is trained for the second time, incorporating additional features derived from the initial classification outcome to enhance the discriminative properties of the relearned decision functions. This strategy bears a conceptual relation to methods such as stacked generalization [41], which integrates information from a prior model outcome for making new predictions.

In our work, we expand on the relearning concept within the framework of a CNN model, which we term as the deep relearning CNN (DRCNN). In this approach, the initial classification outcome from a CNN model is fed into a subsequent CNN model, expanding the input space to guide the learning of discriminative feature representations in an end-to-end manner. We assess the effects of learning the DRCNN cumulatively and non-cumulatively, meaning we extend the input space based on either all previous model outputs or solely the preceding model outputs during an iterative process. Additionally, we integrate the outcome of the DRCNN with an alternative CPP strategy known as object-based voting (OBV). Here, the imagery is segmented using a segmentation algorithm across multiple segmentation layers. The outputs from the DRCNN model are aggregated at segment levels using a majority voting strategy (Fig. 4-5). This approach aims to preserve boundary information of objects that might otherwise be lost or blurred, a common issue in CNN models [42].

As such, our approach introduces a CPP technique based on CNNs for semantic RS image segmentation. Traditional CPP methods aim to improve classification accuracy by enforcing smoothness priors in the image domain. In contrast, our proposed strategy involves a relearning approach, where the initial classification outcome of a CNN model is fed into a subsequent CNN model through an extended input space. As mentioned, this process guides the learning of discriminative feature representations in an end-to-end manner. Further, the DRCNN explicitly considers the geospatial domain by incorporating the spatial alignment of preliminary class labels. We assess the learning of the DRCNN in both cumulative and noncumulative ways—extending the input space based on all previous model outputs or solely the preceding model outputs, respectively—during an iterative procedure. Additionally, the DRCNN can be seamlessly integrated with alternative CPP techniques, such OBV.

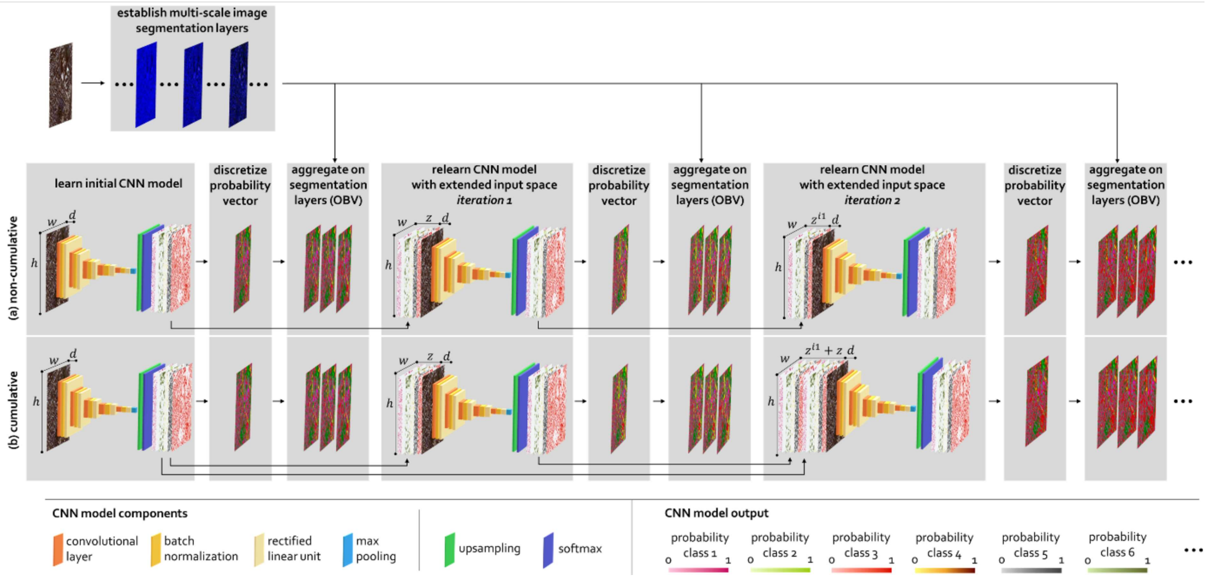

Fig. 4-5. Overview of the proposed DRCNNs. We extracted the content of the figure and caption from [43].

The experimental results obtained from two test sites using WorldView-II imagery underscore the advantageous performance properties of the DRCNN models. These models demonstrate the ability to enhance the accuracies of the initial CNN models, increasing them on average from 72.64% to 76.01% and from 92.43% to 94.52% based on the κ statistic. Furthermore, an additional increase of 1.65 and 2.84 percentage points is achieved when combining the DRCNN models with an OBV strategy. From an epistemological perspective, our results emphasize that CNNs can benefit from considering preliminary model outcomes, and conventional CPP techniques can gain advantages from an upstream relearning strategy.

5. Novel techniques for the characterization of the built environment with EO data

Monitoring settlements is crucial for maintaining up-to-date risk models, particularly concerning exposure. Global urbanization processes and population growth rapidly reshape the Earth's surface, posing a continuous challenge to deliver timely information on the characteristics of built environments. Keeping track of these changes is essential for effective risk assessment and subsequent management.

5.1 Qiu *et al.*, 2020, ISPRS: Large-scale mapping of HSE from Sentinel-2 images

HSE, characterized by buildings, roads, and other man-made structures, serves as a crucial indicator of the human footprint on Earth. In recent years, there was a notable increase in studies focused on HSE mapping, with RS-based approaches gaining attention. RS methods offer the advantage of regular observation of the land surface on a global scale. Several RS-based global products related to HSE emerged. For instance, the Global Urban Footprint was derived using TerraSAR-X and TanDEM-X Synthetic Aperture Radar images [44]. Another product, the global human settlement built-up grid, was derived from Landsat and Sentinel-1 image collections. This grid is a product of the Global Human Settlement Layer image analytics framework, which also incorporates RS images from other missions such as SPOT-5 and 6 [45]. These global products provide valuable insights into the distribution and characteristics of human settlements worldwide.

However, here, our focus is on an automated HSE mapping framework that relies on publicly accessible data, providing high ground sampling distance and continuous measurements across space and time. As a solution, we propose a DL-based framework utilizing a well-generalizing semantic segmentation network. This framework is designed to automatically map HSE using multispectral Sentinel-2 data, with regionally available geo-products serving as training labels. To validate the framework, we compare the results against both manually labeled checkpoints distributed evenly over the test areas and the OpenStreetMap building layer. Extensive comparisons with several baseline products are conducted to thoroughly evaluate the effectiveness of the proposed HSE mapping framework. The mapping capabilities of HSE are consistently demonstrated across 10 representative areas worldwide (Tab. 5-1). Additionally, we present a country-wide HSE mapping example generated by our framework (Fig. 5-1) to showcase its potential for upscaling. The results of this study contribute to the generalization of the applicability of CNN-based approaches for large-scale urban mapping, especially in cases where up-to-date and accurate ground truth data is unavailable.

TAB. 5-1. ACCURACIES OF THE NETWORKS

Method	Test beyond Europe				Test in Europe			
	κ	AA	recall	F1	κ	AA	recall	F1
Sen2HSE (ours)	**0.809**	90.1%	**91.4%**	**0.906**	**0.802**	**90.5%**	**84.4%**	**0.834**
U-Net	0.804	**90.3%**	90.4%	0.903	0.788	89.3%	81.7%	0.822
ResNet-PSPNet	0.655	82.8%	80.3%	0.824	0.644	80.3%	64.5%	0.697
ResNet-FCN-8	0.740	87.2%	89.3%	0.875	0.719	84.8%	73.0%	0.762
FCN+du. att.	0.785	89.4%	86.3%	0.888	0.760	85.2%	72.4%	0.795

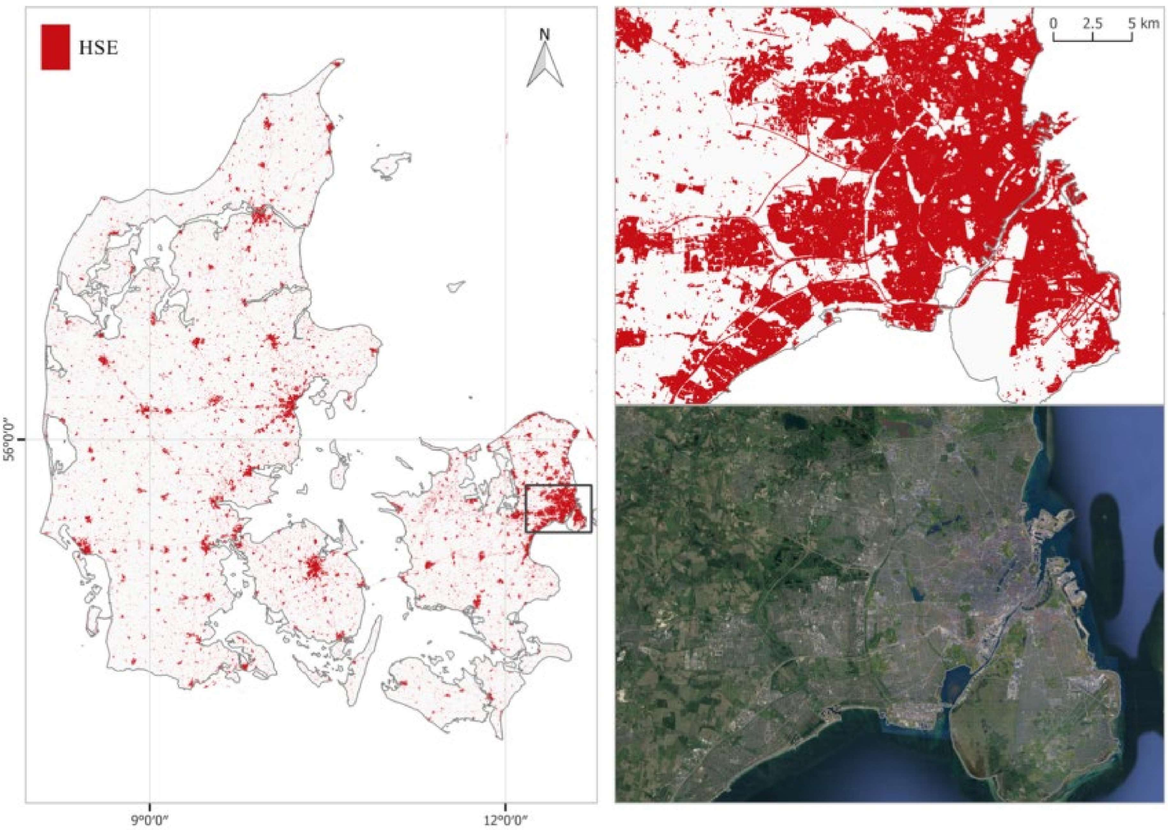

Fig. 5-1. Country-wide HSE mapping example in Denmark. We extracted the content of the figure and caption from [46].

In order to consider three-dimensional properties of built environments, we further propose techniques to compute nDSMs from DSM data, i.e., extract the heights of objects that are elevated from the earth's surface such as built-up structures and vegetation.

5.2 Müller *et al.*, 2023, IEEE JSTARS: Deep Neural Network regression for DSM generation with Sentinel-2

Here, we address the challenge of the unavailability of VHR nDSMs for large areas. To tackle this issue, the focus is on estimating nDSM data from globally available Sentinel-2 imagery. The methodology introduces a process to predict VHR height images at a resolution of 0.5 × 0.5 meters using Sentinel-2 data. Given that Sentinel-2 provides multispectral bands at a lower resolution of 10 × 10 meters, the goal is to investigate whether deep neural networks can effectively bridge this scale difference, which is a factor of 20. To achieve this, a specialized CNN regression architecture is proposed, building upon the U-Net model [47]. The U-Net architecture, known for its success in various scientific fields, is adapted for the task of pixelwise regression, also in the context of satellite imagery [48]. While U-Net is often utilized for segmentation tasks to differentiate between multiple classes of objects, its flexibility extends to pixelwise regression, making it suitable for applications in satellite image interpretation.

The neural network architecture proposed in our study builds upon substantial extensions and enhancements of the U-Net model. In addition to incorporating residual connections, a key innovation is the introduction of a multiscale encoder, addressing the challenge of artifacts on the surface differing in size and shape. This multiscale encoder consists of two parallel encoders with different kernel sizes. By duplicating the encoder with differently sized kernels, i.e., fanning the encoder, we enable the learning of features of varying sizes in each encoder independently. Furthermore, attention mechanisms are integrated when merging the outputs of the different encoders, enhancing the overall model performance. These enhancements not only result in improved numerical accuracies but also yield more coherent visual representations (Fig. 5-2). The outputs can be combined through a mosaic approach to generate nDSM data for larger areas. Overall, our models demonstrate the capability to predict high-resolution nDSM images using lower-resolution optical satellite imagery. Deep neural networks proved effective in managing this leap in scale. Additionally, our findings highlighted the effectiveness of both the multiscale encoder and attention gates developed by us in the specific context of neural network-driven nDSM creation.

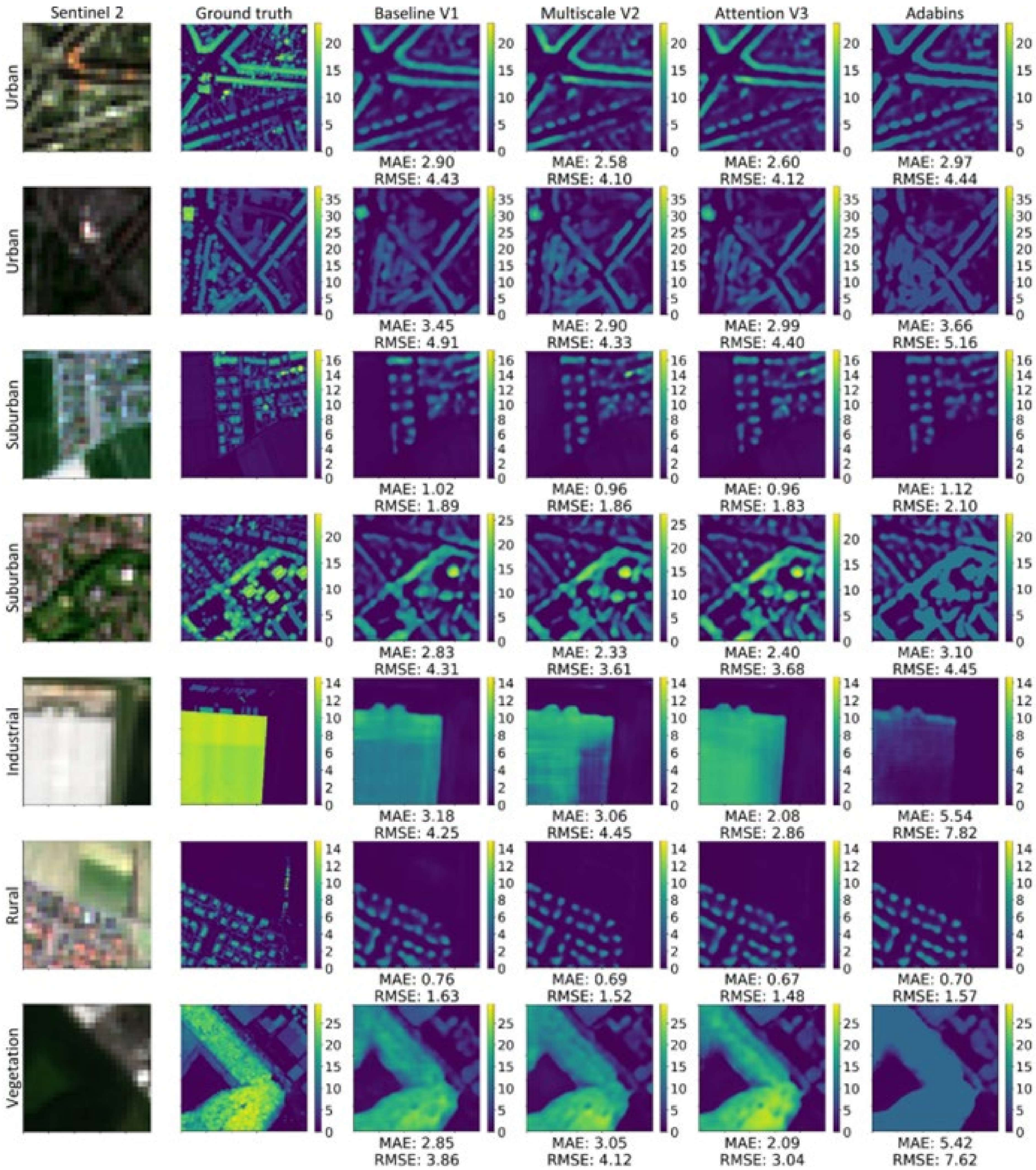

Fig. 5-2. Predictions of our model variants V1-baseline, V2-multiscale, and V3-attention with their input data and ground truth tile, as well as Adabins as a further benchline, respectively. All our models produce decent results despite the lower resolution input data. We extracted the content of the figure and caption from [49].

5.3 Geiß *et al.,* 2020, IEEE GRSL: Training set compilation for DTM generation from the TDM DSM

Subsequently, we address the integration of DSM data for large areas with a high ground sampling distance, leveraging data from the TDM DSM. The TDM is a spaceborne radar interferometer providing a global DSM. Thereby, we aim for an automated DTM generation from TDM DSM data by incorporating additional information from Sentinel-2 imagery and open-source geospatial vector data. The proposed method involves the automatic and robust compilation of training samples by applying specific criteria to the multisource geodata. This compiled data set is then used to train a classification model capable of accurately distinguishing elevated objects from bare earth measurements in the TDM DSM. Subsequently, a DTM is interpolated from the identified bare earth measurements (Fig. 5-3). This workflow enables the integration of TDM DSM data with other geospatial data sets, providing a more comprehensive representation of the terrain.

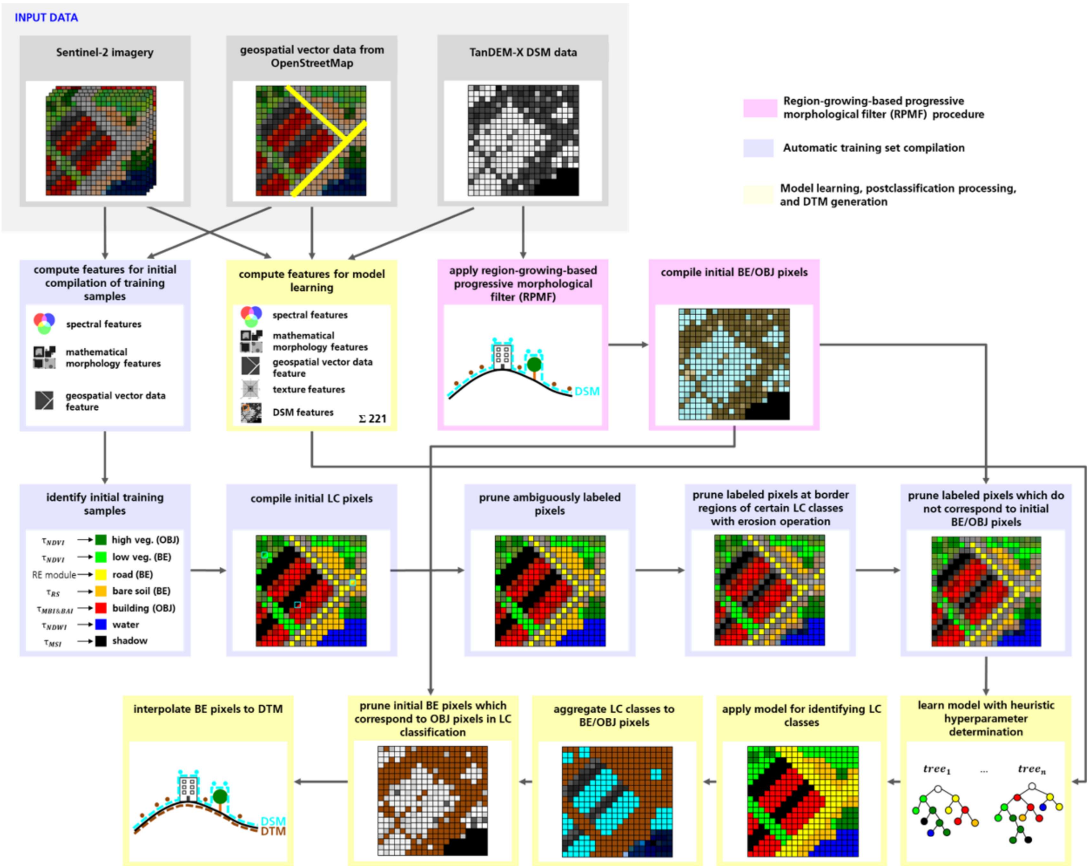

Fig. 5-3. Scheme of the automatic training set compilation approach for DTM generation. We extracted the content of the figure and caption from [50].

The experimental results obtained from a test site covering the complex and heterogeneous built environment of Santiago de Chile, Chile, affirm the effectiveness of the proposed workflow. The workflow demonstrates substantially increased accuracies compared to a morphological filter-based method. This underscores the practical utility and improved performance achieved through the joint consideration of TDM DSM data, Sentinel-2 imagery, and open-source geospatial vector data in the automatic generation of DTMs.

5.4 Geiß *et al.*, 2019, IEEE JSTARS: Large-area characterization of urban morphology

The techniques proposed previously in this section are designed to provide input data for a generic characterization of the built environment. To achieve this, we developed a novel multistep procedure for morphological characterization in terms of built-up density and built-up height. Leveraging elevation measurements from the TDM DSM and multispectral Sentinel-2 imagery, these EO systems strike a balance between relatively high spatial resolution and large-area coverage, enabling spatially continuous analysis of built environments globally. The automated workflow begins with the differentiation of "built-up" and "non-built-up" areas using the Global Urban Footprint processor. This information is then utilized in a tailored filtering procedure for the TDM DSM data to extract elevation information for built-up areas (Fig. 5-4a). Subsequently, intra-urban land cover is mapped based on Sentinel-2 imagery (Fig. 5-4b), providing the foundation for computing built-up densities and built-up heights. Finally, the measures are combined to morphologically characterize the built environment on an ordinal scale of measurement (Fig. 5-4c).

Empirical validation efforts involve a comparative analysis with more than 3.2 million individual building geometries and associated height measurements from cadastral data sources. The data sets cover settlement areas in the capital cities and other major cities in Germany, England, and the Netherlands. Experimental results underscore the capability of morphologically characterizing built environments with viable accuracies. However, they also reveal a systematic underestimation of built-up heights across all morphological classes when compared to reference data. However, adjusting the hyperparameters of the method can mitigate error levels. Consequently, estimations of built-up heights exhibit deviations of approximately 1-2 floors, depending on the specific morphological class. The spatial pattern corresponds well to the distribution of built-up heights in the reference data set. The accuracy of built-up densities is highest in areas with medium built-up heights. On the other hand, lower accuracies are observed in structures with high built-up heights and low densities (resulting in overestimations in intra-urban cores) and in areas with low built-up heights and high densities (leading to underestimations in peripheral or suburban regions of cities). Nonetheless, the majority of morphological classes achieve viable built-up density estimations with deviations of less than 20%. Furthermore, these estimations effectively mirror the general urban morphological structure, features displaying an ideal decrease from the core to the periphery of agglomeration areas. Lastly, in terms of morphological characterization, ordinally weighted global classification accuracy measures consistently show values exceeding 70%, and κ statistics predominantly indicate substantial agreements.

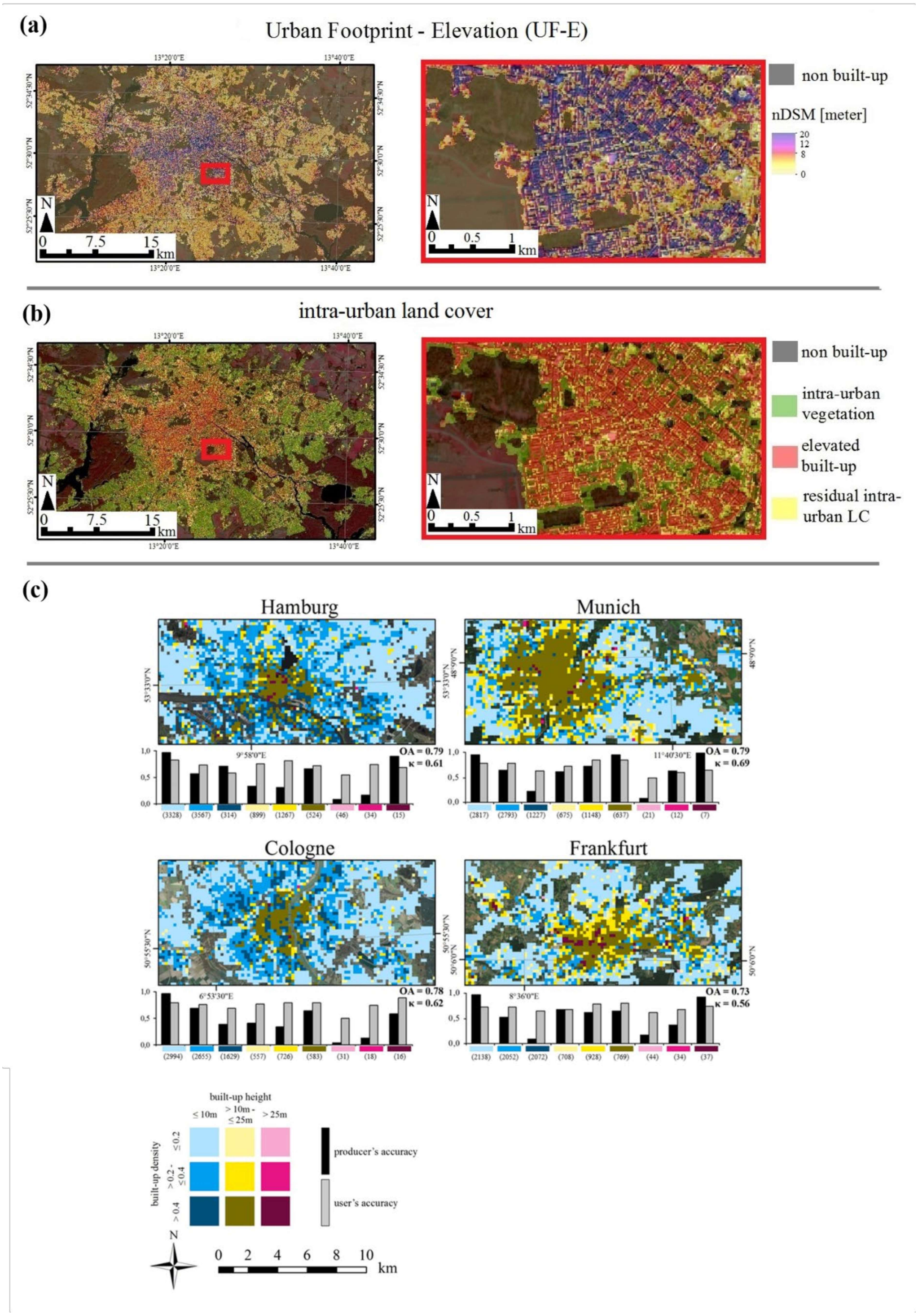

Fig. 5-4. (a) The UF-E model provides intra-urban elevation values. (b) Intra-urban LC map which serve as basis to compute built-up densities and built-up heights. (c) The two measures are combined for a morphologic characterization of the built environment. We extracted the content of the figure and caption from [51].

5.5 Geiß *et al.*, 2020, ISPRS: MSER for mapping of built-up density and built-up height

Nevertheless, despite the consistent global existence of TDM DSM data [52], its accessibility is presently confined to 100,000 square kilometers per data proposal intended for scientific applications. Furthermore, the data undergoes infrequent updates, representing a snapshot at a specific point in time. Consequently, we establish a workflow for estimating built-up density and built-up height using multispectral Sentinel-2 data (Fig. 5-5). To achieve this, we frame the estimation of built-up density and built-up height as a supervised learning problem. Given the rational measurement level of these target variables, the regression estimation problem involves identifying the mapping between an incoming vector, i.e., ubiquitously available features computed from Sentinel-2 data, and an observable output, i.e., training set. This training set is automatically generated from the joint utilization of TDM elevation data and Sentinel-2 imagery, or alternatively, from cadastral sources. The training sets are then employed to regress the target variables for spatial processing units corresponding to urban neighborhood scales.

From a methodological standpoint, we introduce a novel ensemble regression approach termed multistrategy ensemble regression (MSER). This approach is built upon advanced ML-based regression algorithms, including Random Forest (RF) Regression, Support Vector Regression, Gaussian Process Regression, and Neural Network Regression. To establish a robust ensemble, these algorithms are trained using a modified version of the AdaBoost.RT algorithm. However, to ensure diversity among individual boosted regressors reliably, we incorporate a random feature subspace method into the procedure. Unlike existing approaches, we selectively prune non-favorable regressors trained during the boosting procedure and calculate the final prediction using a weighted mean function on the residual models, ensuring improved accuracy properties of predictions. Ultimately, the outputs are combined into a single prediction using a decision fusion strategy.

Experimental results are derived from four test areas encompassing the settlement regions of the four largest German cities: Berlin, Hamburg, Munich, and Cologne. The results unequivocally emphasize the advantageous characteristics of the MSER approach, as all the best predictions were achieved with a boosted regressor in conjunction with a decision fusion strategy in a comparative setup. The mean absolute errors of corresponding models range between 3% and 16% for built-up density and 1–5.4 meters for built-up height, depending on the validation strategy, size of the spatial processing units, and the specific test area. Even in a domain adaptation setup, i.e., learning a model over a source domain area and applying it to a geographically different target domain area, numerous predictions exhibit comparable accuracy levels to those obtained within a source domain. This underscores the feasibility of transferring a learned model to a target domain using the presented framework.

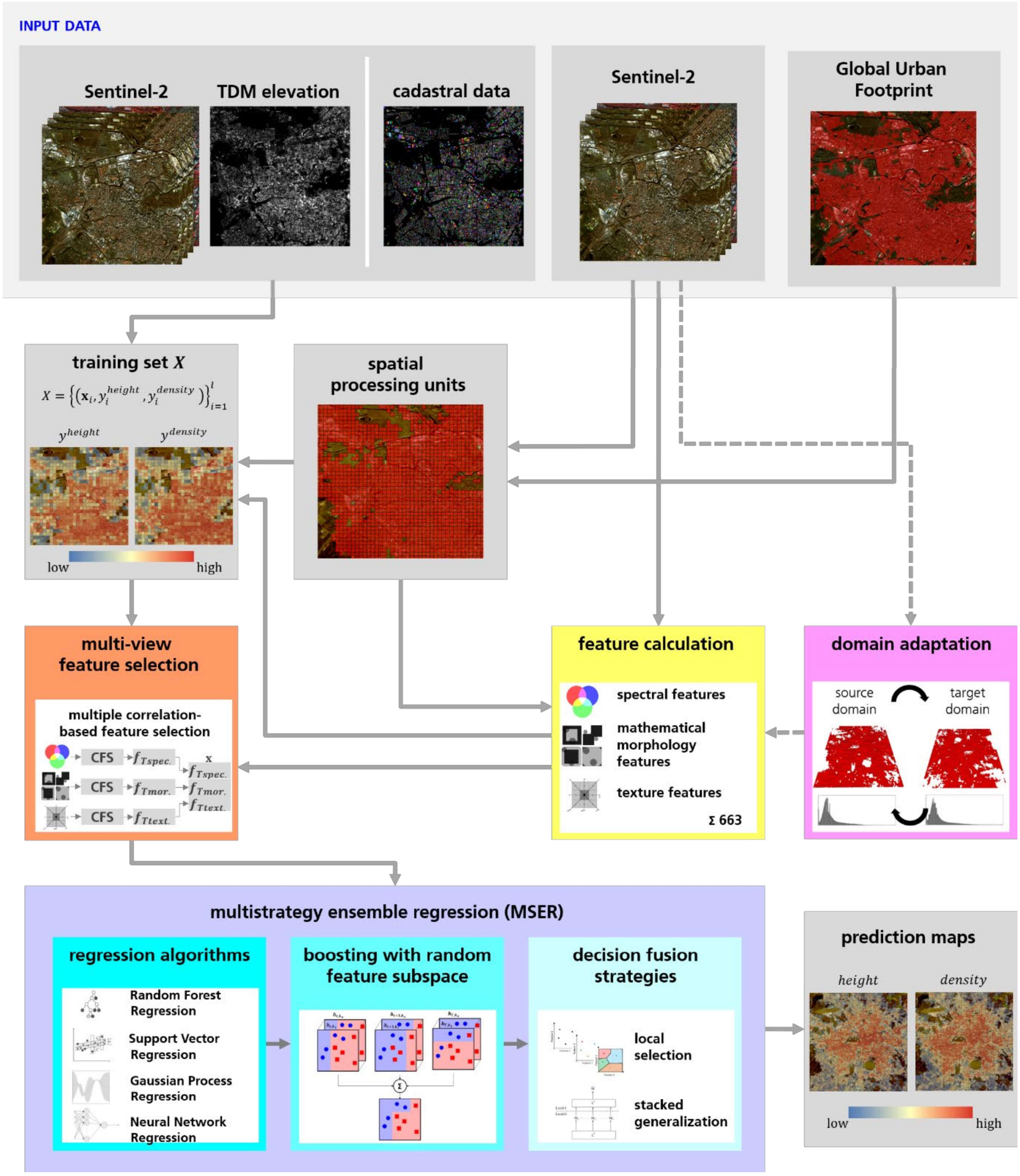

Fig. 5-5. Overview on the input data and processing steps for mapping of built-up density and built-up height. We extracted the content of the figure and caption from [53].

5.6 Geiß *et al.*, 2022, JAG: Multi-target regressor chains with repetitive permutation

The aforementioned supervised learning framework provides a foundation for additional methodological considerations. Multi-task learning techniques offer the advantageous simultaneous estimation of multiple target variables, such as built-up density and built-up height. Thus, here, we introduce a novel multi-task regression (MTR) method termed ensemble of regressor chains with a repetitive permutation scheme. This method belongs to the category of problem transformation-based MTR methods, which involve creating an individual model for each target variable. Subsequently, combining these separate models allows for obtaining an overall prediction. Our approach is built upon the concept of an ensemble of regressor chains, aligning single-target models along a flexible permutation, i.e., chain. To specifically address situations with a small number of target variables, we enhance regressor chains with a repetitive permutation scheme. Estimates of the target variables cascade to subsequent models as additional features when learning along a chain, allowing one target variable to occupy multiple elements of the chain (Fig. 5-6).

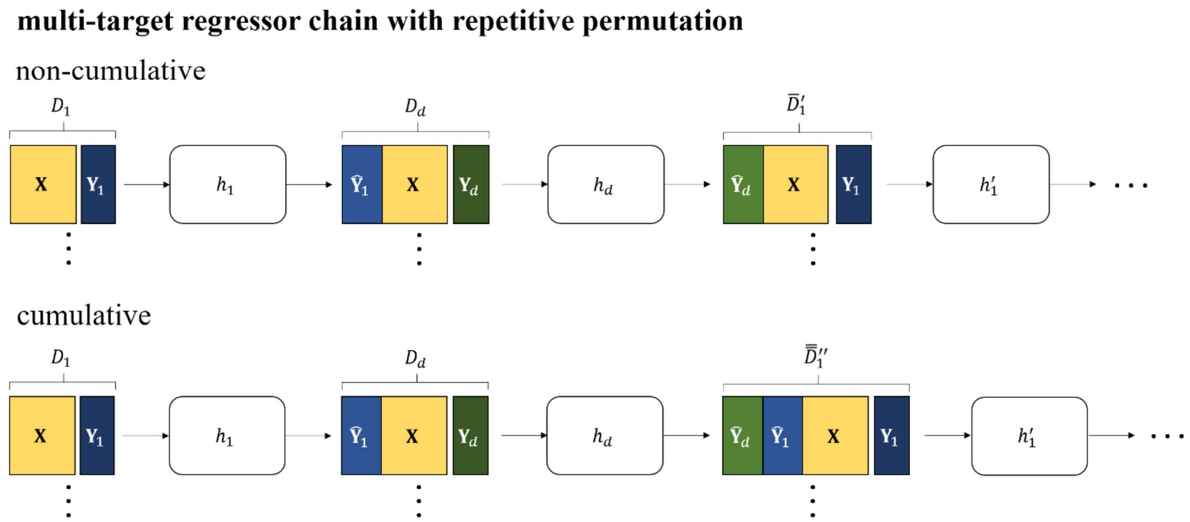

Fig. 5-6. Illustration of the training procedures of ensemble of regressor chains with repetitive permutation with a non-cumulative and cumulative augmentation strategy of the feature vector, respectively. We extracted the content of the figure and caption from [54].

We conduct an experimental evaluation of the method by simultaneously estimating built-up density and built-up height using features derived from Sentinel-2 data for the four largest cities in Germany within a comparative framework. We explore single-target stacking, multi-target stacking, and ensemble of regressor chains without repetitive permutation alongside our proposed method. The empirical results underscore the advantageous performance properties of MTR methods. Specifically, our ensemble of regressor chains with a repetitive permutation scheme consistently achieved the highest accuracies compared to the other MTR methods. Across the experiments, it yielded mean improvements of 14.5% compared to the initial single-target models.

5.7 Geiß *et al.*, 2022, Array: Source domain selection for domain adaptation in RS

In the realm of supervised learning techniques, leveraging existing prior knowledge from a source domain to estimate a target variable in a target domain through domain adaptation is often desirable. This helps mitigating the need for costly compilation of training data in the target domain. Domain adaptation typically involves addressing two subproblems: covariate shift and sample selection bias. Sample selection bias occurs when the nature of observed objects changes between the source and target domains, making source domain samples non-representative for the unlabeled target domain samples. Covariate shift is a specific case of sample selection bias induced by changes in independent variables, frequently seen in RS due to variations in data acquisition properties such as illumination and acquisition angle.

Ensuring a viable model transfer from a source to a target domain, where the domains are related, is crucial. We tackle this situation by carefully selecting the source domain from which the model should be learned before transferring it. Our aim is to efficiently adapt to a target domain when multiple potentially helpful but unlabeled source domains exist. Consequently, we propose unsupervised source selection by voting from similarity metrics on aligned marginal distributions of image features in source and target domains. Additionally, we introduce an unsupervised pruning heuristic to include solely robust similarity metrics in an ensemble voting scheme (Fig. 5-7).

We evaluate these methods by training models on Level-of-Detail-1 building models and regressing built-up density and built-up height on Sentinel-2 satellite imagery. To assess the domain adaptation capability, we interchangeably learn and apply models for the four largest cities in Germany. Experimental results highlight the methods' ability to achieve higher accuracy levels more frequently, with improvements of up to 10% using the most robust selection mechanisms compared to random source-target domain selections.

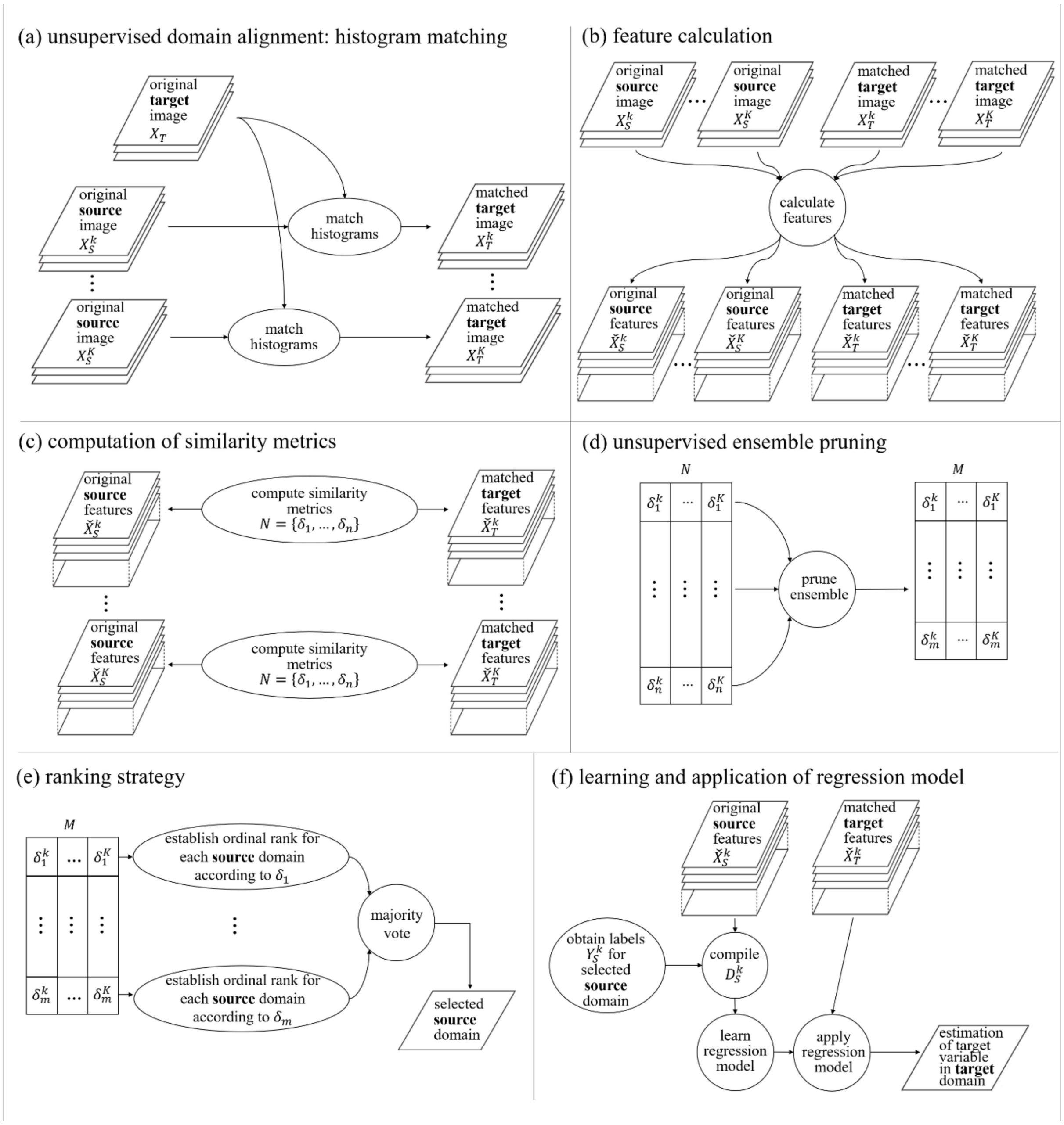

Fig. 5-7. Overview of the individual processing steps for optimized source domain selection in a domain adaptation context. (a) A histogram matching procedure aligns the shapes of the histograms of the spectral bands of the satellite imagery which covers a target domain to the spectral bands of the satellite imagery which cover the potential source domains individually. (b) The matched data is deployed for computing an exhaustive set of spectral-spatial features. (c) The features are deployed to compute a variety of similarity metrics. (d) An ensemble pruning strategy aims for identifying a robust subset of similarity metrics. (e) The selected similarity metrics are used to evaluate all possible source-target domain combinations and identify the combination which is most similar. The identified combinations from the similarity metrics are combined via a majority voting strategy. (f) Labeled samples are obtained for a selected source domain and a regression model is learned from the corresponding source image features and applied to estimate the target variable in the target domain. We extracted the content of the figure and caption from [55].

6. Exposure modelling for natural hazard risk assessment

Exposure plays a crucial role in risk models, representing elements that are endangered by a hazard and susceptible to damage. Vulnerability, on the other hand, assesses the likelihood of experiencing damage, translating into potential losses, at varying levels of hazard intensity. Often, compiling exposure information is the most resource-intensive aspect of risk assessment procedures, both in terms of time and labor. Traditional models frequently describe exposure in a spatially aggregated manner, relying on statistical or census data for specific administrative entities. In this section, we introduce novel top-down and bottom-up exposure assessment procedures based on modern EO systems and innovative data sources such as street-level imagery.

6.1 Geiß *et al.*, 2023, NatHaz: Benefits of EO for disaggregation of exposure and earthquake loss modelling

Modern EO techniques, such as the TDM and Sentinel-2 mission, provide spatially continuous information for large geographic areas with high geometric resolution. In our approach, we leverage EO data to characterize the built environment in terms of morphologic properties, specifically built-up density and built-up height. Subsequently, we employ this information to enhance existing exposure data through a spatial disaggregation approach, utilizing dasymetric methods (Fig. 6-1). First, EO-based built-up height measurements are classified into distinct building height classes, aligning with predefined height classes of building structural types. The classification, based on relative height thresholds, precisely reproduces the distribution of height classes at the so-called comuna level (administrative entities). These classifications determine the potential structural types in a given grid cell (up to nine types per cell). Additionally, living areas per building height class are aggregated at the comuna level.

The sum per specific building height class is then redistributed over grid cells corresponding to that class while maintaining the characteristic shares of individual structural types within the class. Finally, built-up density is employed to disaggregate living areas in a weighted manner, redistributing living areas per building height class proportionally based on corresponding built-up densities. For further use, the mapped living area per building type is divided by corresponding average living areas per building type, as defined in the deployed national exposure model for Chile [56], to obtain the absolute number of buildings per type.

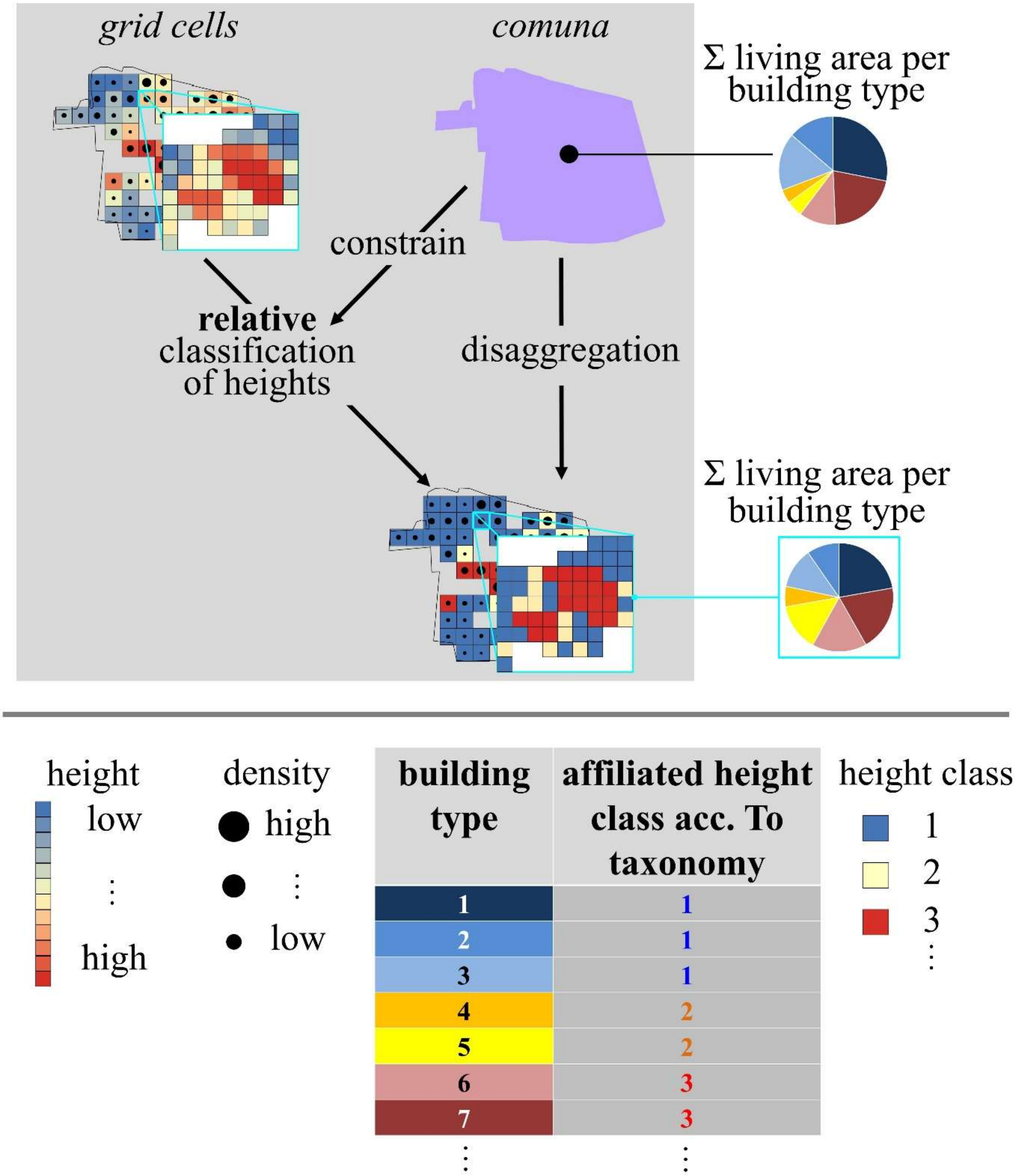

Fig. 6-1. Proposed exposure disaggregation technique using estimated built-up height and built-up density data from EO. We extracted the content of the figure and caption from [56].

The study area focuses on the city of Santiago de Chile, a region susceptible to hazards, particularly earthquakes. The findings include loss estimations resulting from seismic ground shaking, along with corresponding sensitivity analyses based on the resolution properties of the exposure data used in the model (Fig. 6-2). The results underscore the advantages of leveraging modern EO technologies for detailed exposure mapping and associated earthquake loss estimation, demonstrating improved accuracy properties in the assessments.

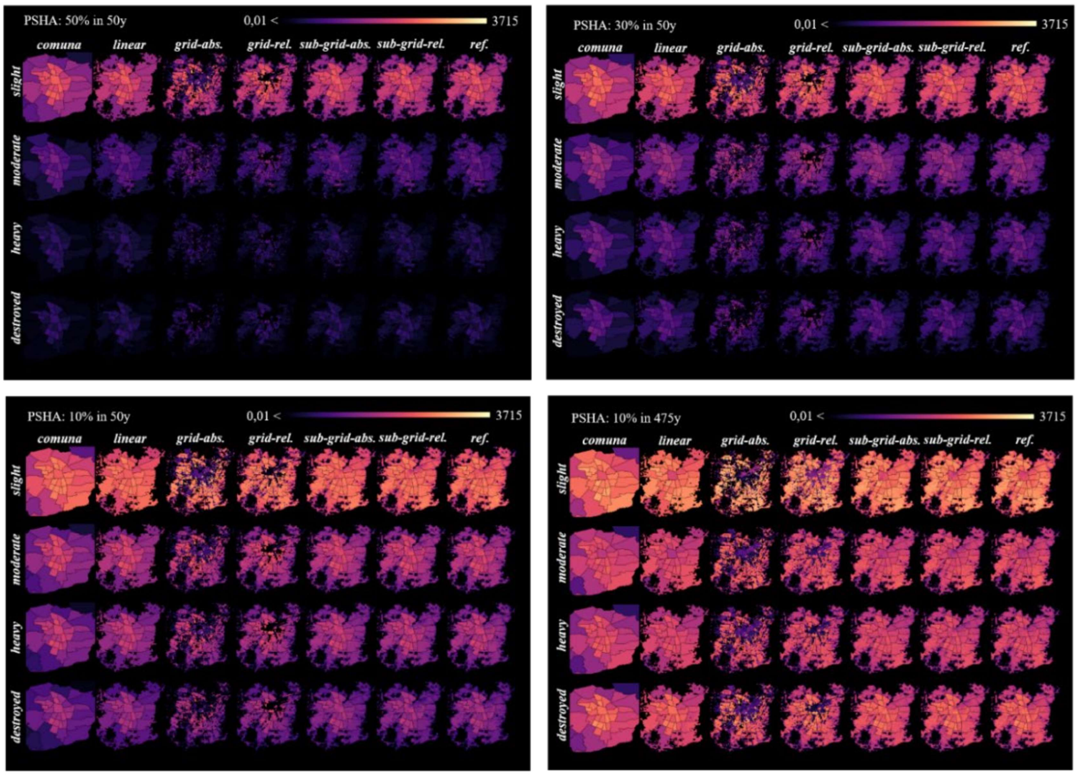

Fig. 6-2. Results of the different mapping techniques regarding the four building damage states and probabilistic seismic hazard assessment (PSHA) results. The color bars indicate the absolute number of buildings per grid cell according to a certain damage state and PSHA result, respectively. It can be traced how the number of damaged buildings increases with increasing intensity of shaking. Thereby, large parts of the business and financial areas, which expand northeastwards from the city center, feature a comparatively low concentration of damaged buildings. Generally, the underlying mechanism relates to the existence of high-rise buildings in the city center, which are typically compliant with seismic design provisions and thus, having low fragility. In contrast, particularly for the considered severe events, i.e., earthquakes with a probability of occurrence of 10% within 50 years and with 10% in 475 years, respectively, we observe that large areas at the fringes of the city might feature a high concentration of damaged buildings, which relates to the existence of numerous low-rise building types with a comparative higher seismic fragility (e.g., informal, non-engineered structures). We extracted the content of the figure and caption from [56].

6.2 Aravena Pelizari *et al.*, 2021, ISPRS: Building characterization using street-level imagery and DL

As previously mentioned, accurate seismic risk modeling necessitates knowledge of key structural characteristics of buildings. However, the collection of such data is expensive in terms of financial resources and time, making it impractical for large-scale continuous monitoring. This study quantitatively assesses the potential for an automated and more efficient collection of vulnerability-related structural building characteristics using deep CNNs and street-level imagery, such as that provided by the Google Street View platform. The proposed approach involves a customized hierarchical categorization workflow to organize the highly diverse street-level imagery in an application-oriented manner. Subsequently, state-of-the-art deep CNNs are employed to automate the inference of Seismic Building Structural Types (SBSTs) (Fig. 6-3a), which reflect a building's main-load bearing structure and, consequently, its resistance to seismic forces. In addition, we evaluate the independent retrieval of two key building structural parameters: the material of the lateral-load-resisting system and building height, aiming for a more generic structural characterization of buildings. Supervised learning, particularly with deep CNNs, relies on a sufficient number of labeled training data to result in well-generalizing models. However, consistent ground truth data at the building level for our target variables is often scarce and unavailable. Therefore, we compile reference data based on remote rapid visual screening. Assigning buildings with structural attributes based on their façade views is not straightforward, as discriminative information regarding structural properties, such as the material of the lateral load-resisting system, can be subtle in a façade view. Thus, specific knowledge about the impact of construction practices on the visual appearance of buildings—distinct dependencies between structural properties and visually inferable indicators, referred to as visual-structural criteria—is required for reliable labeling. To facilitate this, we structured such information and developed a scheme that aims to be both representative in terms of occurring construction types and vulnerabilities and to address the needs of training and evaluating deep CNNs.

It is worth noting that numerous taxonomies were developed to categorize building exposure in a standardized manner [57]. In this study, we align the addressed typologies with the Global Earthquake Model (GEM) building taxonomy [58] (referred to as the GEM taxonomy). Consequently, we create a reference data set based on which we evaluate the potential of deep CNNs to predict risk-oriented SBSTs. This enables the linking of buildings to a specific vulnerability model. Additionally, we individually estimate the material of the lateral-load-resisting system and the height of buildings. This is done to exemplify the automated collection of specific attributes within generic faceted data schemes [57], such as the GEM or the GED4ALL taxonomy (adapted for multi-hazard risk analysis [59]).

In conclusion, we showcase the large-area characterization of buildings using a sample of over 200,000 façade images evenly distributed across our test site, the earthquake-prone metropolis of Santiago de Chile, Chile (Fig. 6-3b). The experimental evaluation demonstrates accuracies surpassing κ statistic of 0.8 for all the classification tasks addressed. This underscores the potential of the proposed methodology for efficient *in-situ* data collection on large spatial scales, intended for risk assessments related to earthquakes and other natural hazards, such as tsunamis or floods.

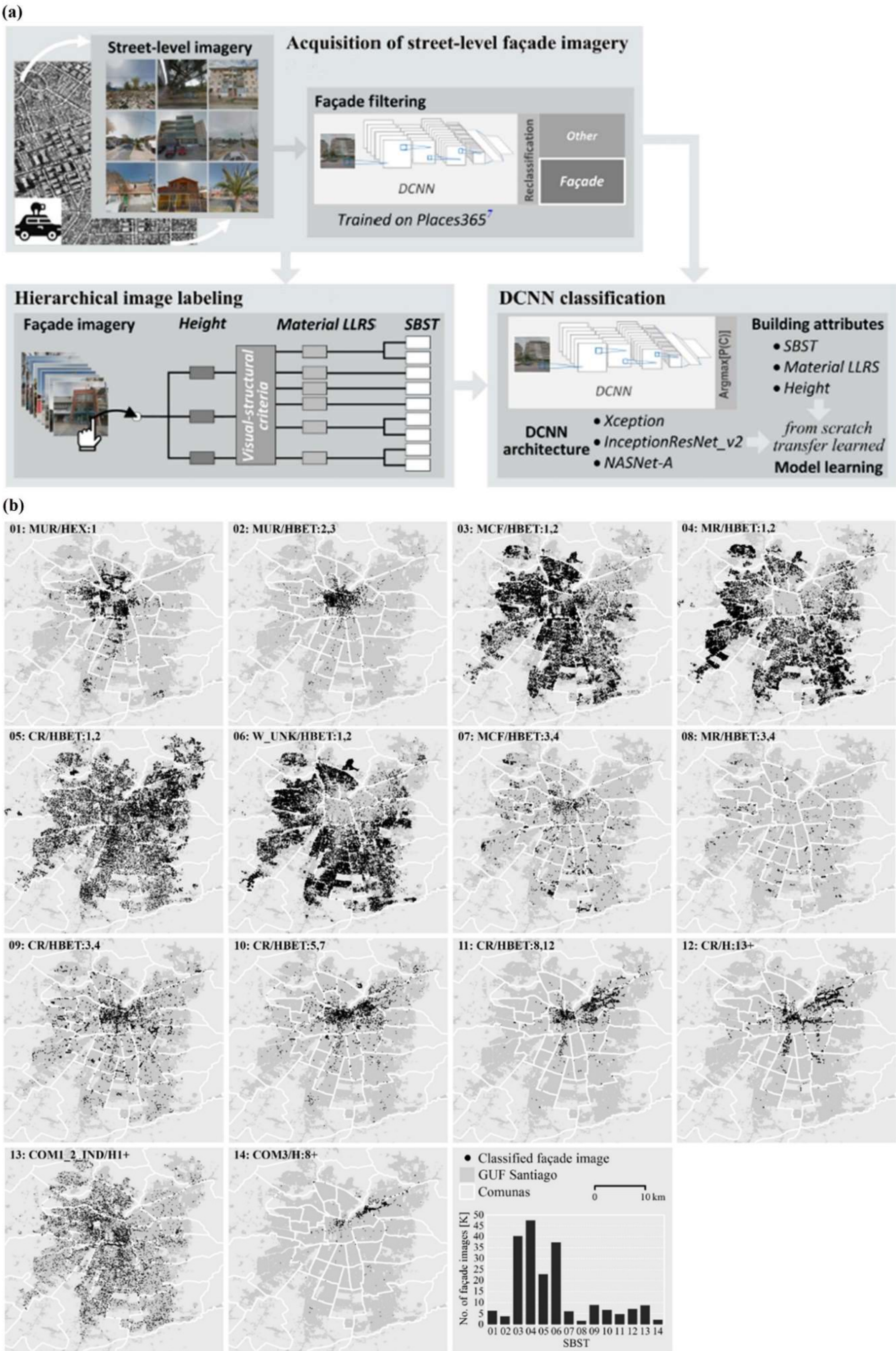

Fig. 6-3. (a) Workflow and (b) distribution of SBSTs. We extracted the content of the figure and caption from [60].

6.3 Aravena Pelizari *et al.*, 2023, ISPRS: Deep multitask learning with label interdependency distillation

To build upon prior research in the realm of multiple hazards, our objective is to focus on a specific classification system, such as the GED4ALL multi-hazard building classification system introduced by Silva et al. [61]. This system not only encompasses risk-oriented SBSTs but also includes the lateral load-resisting system (i.e., the structural mechanism countering lateral forces such as seismic loads, wind loads, water pressure, or earth pressure) along with considerations of material (e.g., masonry or wood), height, occupancy, building plan shape, structural irregularity, roof shape, etc. Methodologically, we adopt multitask learning to tackle this challenge. Multitask learning seeks to concurrently address multiple prediction problems by leveraging shared information across diverse tasks. However, to avoid overlooking crucial information due to interdependencies, we present a novel deep multitask learning architecture tailored to capture cross-task interdependencies within the context of multiple image classification challenges. The architecture involves an intermediately supervised hard parameter sharing CNN providing task-wise interim class label probability predictions. Interdependencies are inferred in two ways: i) by directly integrating label probability sequences into the image feature vector (referred to as multitask stacking), and ii) by transmitting probability sequences to gated recurrent unit-based recurrent neural networks. This enables the explicit learning of cross-task interdependency representations, which are then stacked onto the image feature vector (referred to as interdependency representation learning). This proposed multitask learning architecture (Fig. 6-4a) serves as a tool for comprehensive building characterization using street-level imagery, particularly in the context of risk assessments for various natural hazards.

Experimental outcomes related to the classification of buildings in Santiago de Chile based on five vulnerability-related variables (height, lateral load-resisting system material, SBST, roof shape, and block position) are presented in Fig. 6-4b. Our multitask learning approaches consistently surpass both single-task learning and traditional hard parameter sharing models. Even when starting with high initial classification accuracy, the estimated generalization capabilities show significant improvement, with accumulated task-specific residuals exceeding +6% κ. The combination of multitask stacking and interdependency representation learning achieves the highest accuracy estimates for this task and data setting, with cross-task accuracy mean values reaching 88.43% overall accuracy and 84.49% κ. Notably, from an efficiency standpoint, the proposed multitask methods prove to be notably advantageous compared to single-task learning in terms of training time consumption.

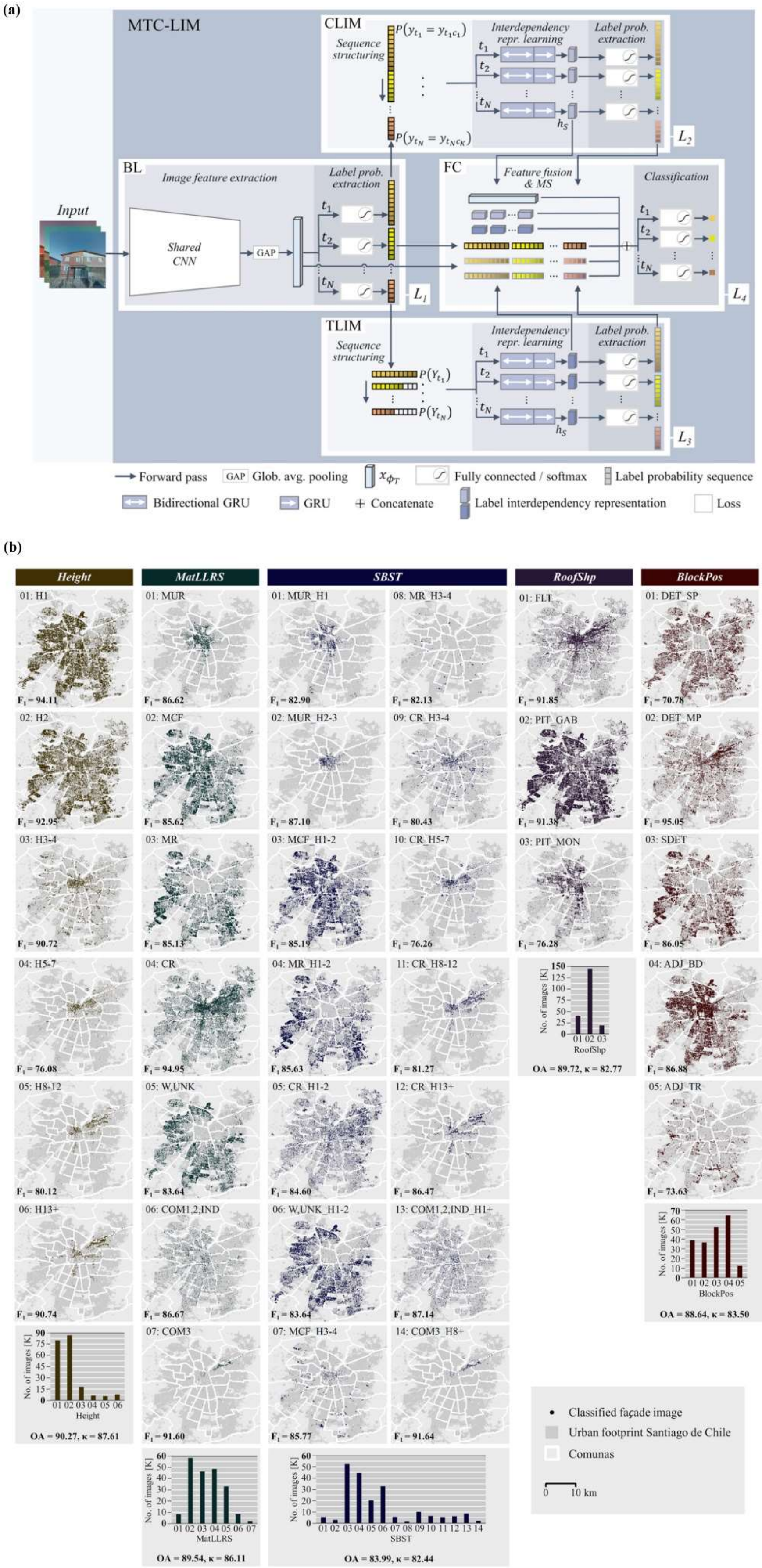

Fig. 6-4. (a) Multitask model and (b) predictions. Content of the figure and caption extracted from [62].

6.4 Liuzzi *et al.*, 2019, BullEQ: A transferable RS approach to classify building structural types

Here, our focus extends to transferable methods for characterizing the built environment. We introduce a methodology utilizing ML algorithms for the swift and robust classification of structural types in buildings from multispectral RS imagery. The primary objective is to evaluate the seismic vulnerability of buildings, with a specific emphasis on the transferability of the developed models. As mentioned previously, the seismic performance of buildings is significantly influenced by structural characteristics such as material composition, age, height, and other key structural features. In this context, we present a methodology designed for transferability, specifically addressing scenarios with imbalanced *in-situ* data. Imbalance refers to a substantial discrepancy in the number of labeled samples available for model learning across different structural types. Our approach involves constructing a transferable model that identifies domain-invariant features from a comprehensive set. This design minimizes sensitivity to domain adaption challenges often arising from variations in acquisition parameters in RS imagery. The key finding is that a limited set of geometry features exhibits generalization capabilities comparable to models generated with a larger number of features describing spectral, geometrical, or contextual building properties. Our study leverages an extensive geodatabase containing nearly 18,000 building footprints. We employ a feature selection strategy based on RF to objectively identify the most valuable features for prediction. Furthermore, we address the issue of imbalanced classes through two approaches: downsampling the majority class and internally modifying the classifier using a weighted RF approach.

The model we developed is applied to the complex urban morphology of the Val d’Agri area in Italy (Fig. 6-5). Italy experienced devastating seismic events over the past 50 years, resulting in more than 5000 casualties and economic losses exceeding 120 billion €. These alarming figures underscore the considerable vulnerability of urban systems to earthquakes. To effectively mitigate this risk, it is imperative to reduce the vulnerability of structures through earthquake-resistant design for new constructions and, particularly, by implementing strengthening measures for existing ones. The destructive events in Italy in 2016 underscore the urgent need for a comprehensive vulnerability assessment in the region. The study's results affirm the statistical robustness of our model and underscore the significance of geometric features. These features enable the reliable identification of structural types, aiding in the identification of potential damage hot spots.

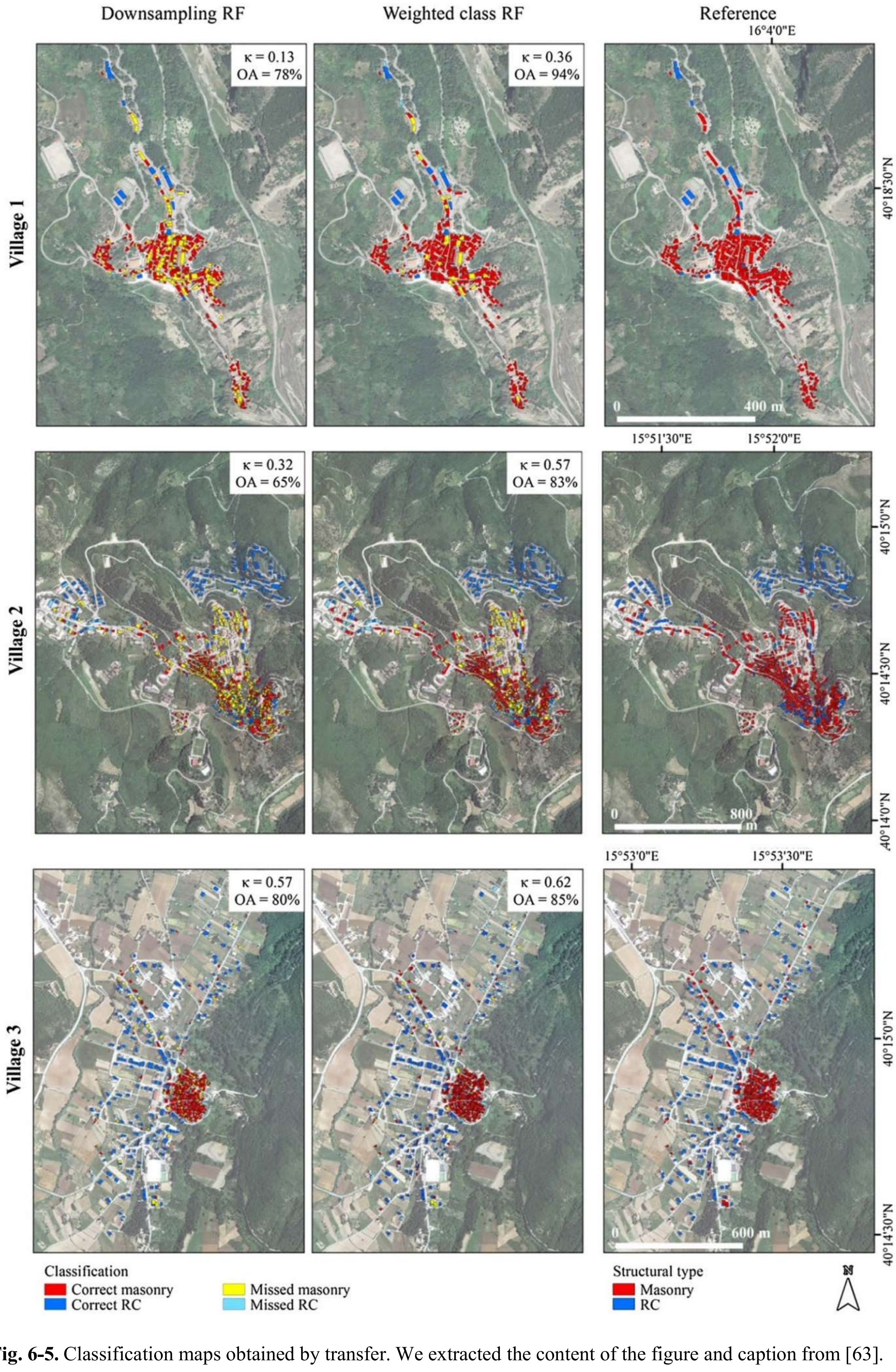

Fig. 6-5. Classification maps obtained by transfer. We extracted the content of the figure and caption from [63].

6.5 Kühnl *et al.*, 2022, NatHaz: Multitemporal landslide exposure and vulnerability assessment

Information about exposure is crucial not only for seismic events but also for assessing risks related to other natural hazards. Landslides, in particular, are frequent and often deadly natural hazards, typically associated with steep slopes and specific loose soil types. Additionally, in the context of climate change, the likelihood of extreme weather events, such as heavy rainfall that can trigger landslides, is on the rise. Additionally, highly dynamic urbanization processes are frequently accompanied by the creation of informal urban settlements. These processes are driven by increasing population numbers and the expansion of settlements: economically disadvantaged population groups often find themselves with no alternative but to build informally in high-risk areas, despite the known perils. This creates a challenge where the urgency of housing needs and rapid urban expansion can override the cautious consideration of hazard risks.

Against this backdrop, we conduct a systematic examination of how risks evolve over a 24-year period, spanning from 1994 to 2018. Our focus is on citywide exposure and, more specifically, on different social groups. To achieve this, we utilize diverse input data from RS, landslide hazard maps, and census data. Our case study is the city of Medellín in Colombia. Employing a set of integrated methods, we map, quantify, and monitor exposure and social vulnerability at a fine spatial granularity (Fig. 6-6a-c). Our findings highlight the dynamic growth in both total population and urban areas over the examined period. However, we observe that the city's expansion is socially uneven. Areas with higher social vulnerability, as indicated by informal settlements, are disproportionately located in regions exposed to landslides (Fig. 6-6d). Notably, we identify a consistent increase each year in settlement areas and people exposed to landslide hazards. Over the period from 1994 to 2018, the total number of socially vulnerable individuals at risk doubled. Despite recent years seeing an increase in the share of the population in formal settlements within hazardous landslide areas, the majority of such areas continue to be occupied by socially vulnerable populations. In conclusion, this study proposes a methodological setup that allows for monitoring exposure and social vulnerability over long time spans at a fine spatial resolution, that brings inequality into the spotlight, and that provides decision-makers with information to develop socially responsible policies.

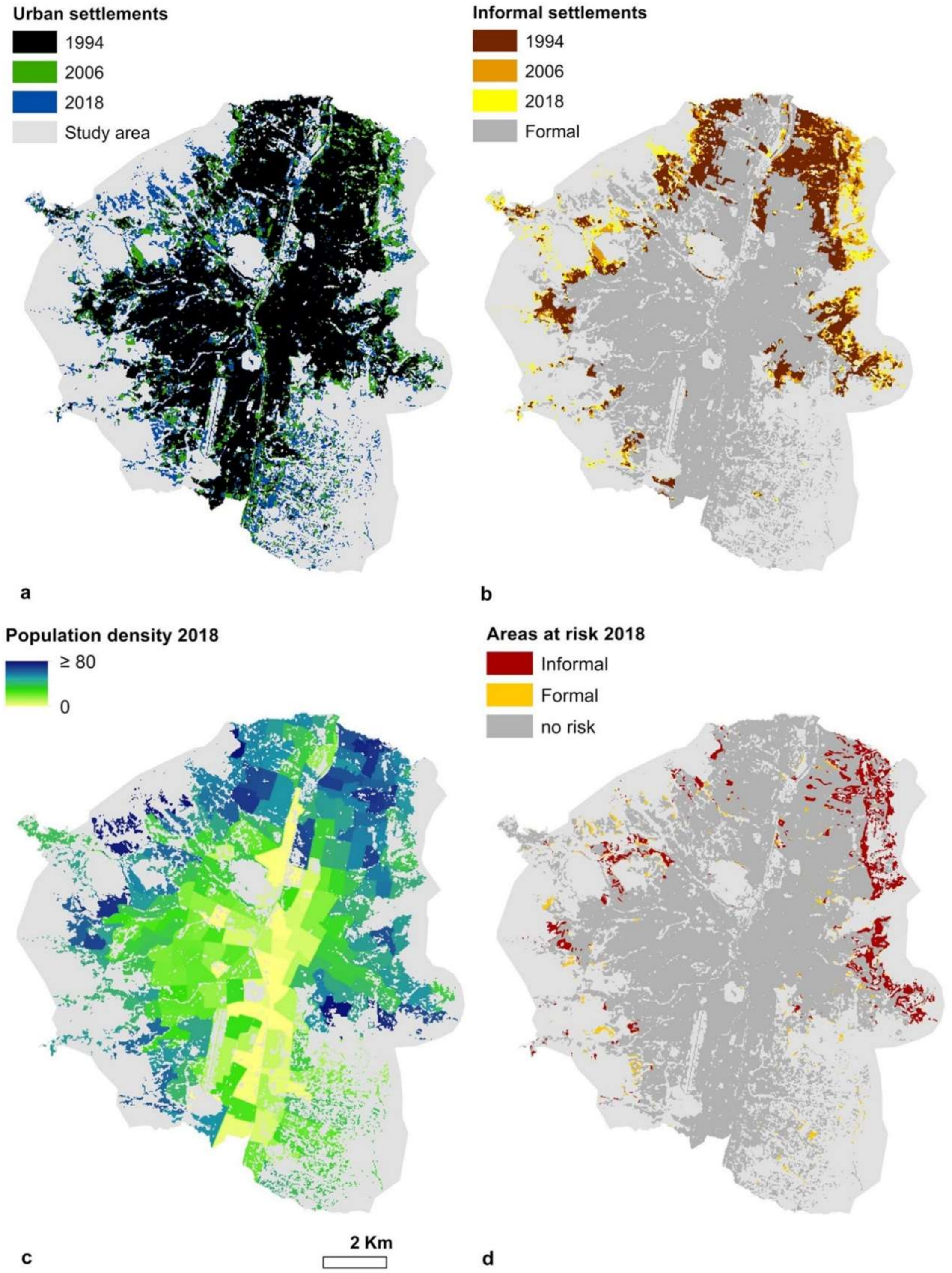

Fig. 6-6. (a) Urban settlement masks 1994–2018 extracted from the Land Cover (LC) classifications implemented with Landsat data. The urban settlements include formal and informal areas of the city. (b) Informal urban settlement masks 1994–2018 calculated based on the informal settlement mask 2019 and the urban settlement masks 1994–2018 based on the LC classifications. (c) Population estimation 2018 per pixel in the extent of the urban settlement mask 2018 through disaggregation and extrapolation based on the census 2018. Since the estimates are based on census data, their administrative boundaries are still visible to a certain extent. (d) The spatial distribution of areas at risk in Medellín for the year 2018 was determined. These areas were categorized based on their social vulnerability status, which was approximated by considering formality and informality. We extracted the content of the figure and caption from [64].

7. Post-event damage assessment

RS techniques stand out as the sole data collection mechanisms capable of providing spatially continuous measurements for extensive areas immediately following the occurrence of a disaster [65]. To assess the condition of the built environment, such as distinguishing between "undamaged" and "damaged/destroyed" buildings, ML techniques are extensively employed in this application domain, owing to their robust information extraction capabilities. Numerous previous applications of ML in RS demonstrated success in identifying damaged buildings in the aftermath of large-scale disasters. However, it is important to note that standard methods often overlook the complexity and associated costs of compiling a training data set after the onset of a disaster event.

7.1 Moya *et al.*, 2021, IEEE TGRS: Intensity-based selection of samples for RS damage assessment

In this study, we focus on disaster events where intensity can be accurately modeled through numerical simulation or instrumentation. For such cases, we introduce two fully automatic procedures designed for the detection of severely damaged buildings. The underlying assumption is that areas with low disaster intensity primarily consist of undamaged buildings. Conversely, areas with moderate to strong disaster intensities likely contain both damaged and undamaged buildings. Given this assumption, the first procedure employs automatic sample selection for learning and calibrating the standard SVM classifier. This method, referred to as distance-based sample selection, is illustrated in Fig. 7-1a-c. The second procedure involves the use of two regularization parameters to define SVs, referred to as multiple regularization parameter approach, as depicted in Fig. 7-1d-f. Both procedures aim to enhance the accuracy of identifying severely damaged buildings in the aftermath of disaster events with modeled intensity.

These frameworks eliminate the need for collecting labeled building samples through field surveys or visual inspection of optical images, processes that are time-intensive. The effectiveness of the proposed method is assessed through application to three real cases: the 2011 Tohoku-Oki earthquake–tsunami, the 2016 Kumamoto earthquake, and the 2018 Okayama floods. The achieved accuracy in these cases ranges between 0.85 and 0.89, indicating that the results are suitable for the swift identification of affected buildings.

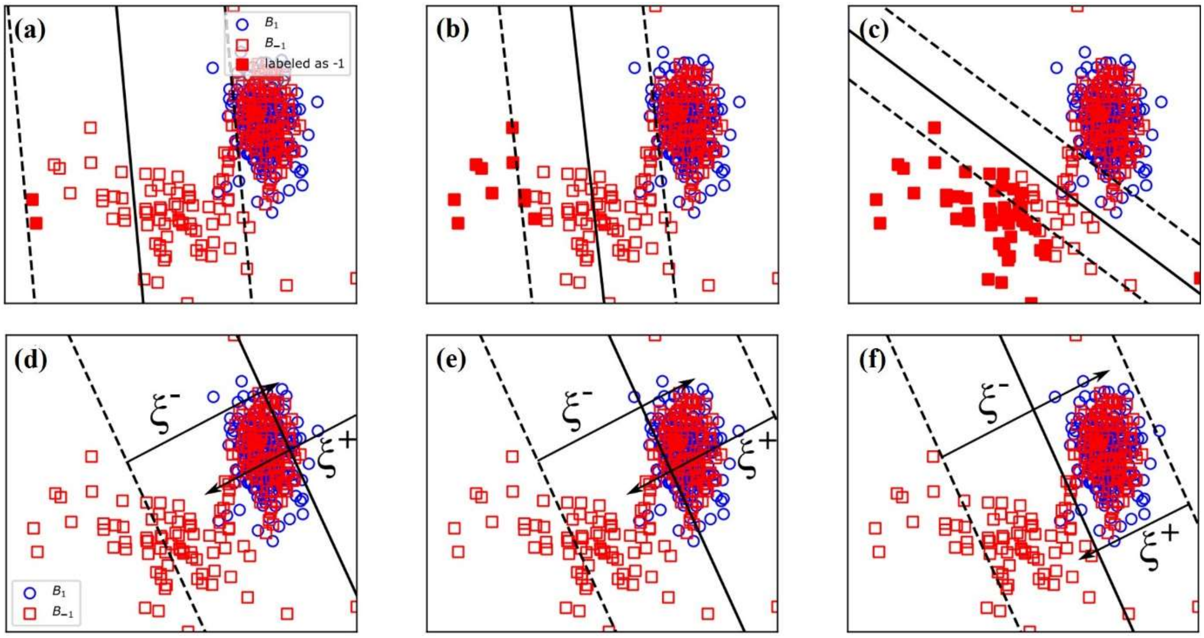

Fig. 7-1. Functionality and sensitivity evaluation of the two proposed methods, i.e., distance-based sample selection and multiple regularization parameter approach. Discriminant function (solid line) and margin bounds (dashed lines) at different stages of the distance-based sample selection approach. Blue circles: samples from B_1. Red squares: samples from $B_{-1}(\#B_1 = \#B_{-1} = 200)$. The filled squares are the samples that belong to $\hat{B}_{-1}$ when (a) $\#\hat{B}_{-1} = 2$, (b) $\#\hat{B}_{-1} = 10$, and (c) $\#\hat{B}_{-1} = 50$. Multiple regularization parameter approach: effect of the parameters λ_p and λ_n in the calibration. Boundary decision function computed for (d) $\lambda_p/\lambda_n = 0.5$, (e) $\lambda_p/\lambda_n = 1.0$, and (f) $\lambda_p/\lambda_n = 2.0$. The solid line denotes the boundary decision function $h(x) = 0$. The dashed lines denote the bounds of the margin. The arrows denote the largest slack variable for $B_1(\xi^+)$ and $B_{-1}(\xi^-)$. Note that the smallest value of ξ^- occurs when $\lambda_p/\lambda_n = 0.5$, whereas the smallest value for ξ^+ occurs when $\lambda_p/\lambda_n = 2.0$. We extracted the content of the figure and caption from [66].

8. Anticipating a risky future

To anticipate future exposure patterns using EO-based time series data, we first develop a customized processing pipeline with three key components: i) we implement innovative super-resolution imaging techniques to enhance the spatial resolution of time series data. This is particularly crucial for data sets with long temporal coverage, such as Landsat, where the spatial resolution properties are frequently limited. ii) We introduce a new classification framework specifically designed for handling time series data. iii) Lastly, we devise a DL-based framework for accurate geospatial extrapolation of time series data. This component leverages the capabilities of DL to provide precise predictions and extend insights into geospatial trends.

8.1 Zhu *et al.*, 2021, JAG: Image super-resolution for multi-temporal RS image classification

Image super-resolution techniques offer substantial benefits for RS, especially in extracting thematic information from imagery. This becomes particularly crucial for image classification based on time series data, where RS data sets with extended temporal coverage often suffer from limited spatial resolution. Recent advancements in DL opened up new possibilities for improving the spatial resolution of historical RS data. While many CNN-based methods demonstrated superior performance in developing end-to-end super-resolution models for natural images, their application in promoting image classification based on multispectral RS data was relatively underexplored. In response, we introduce a novel CNN-based framework designed to enhance the spatial resolution of time series multispectral RS imagery. Our proposed super-resolution model utilizes Residual Channel Attention Networks as a backbone structure. Building upon this architecture, our models uniquely integrate tailored channel-spatial attention and dense-sampling mechanisms to improve performance. Subsequently, state-of-the-art CNN-based classifiers are integrated to generate classification maps based on the enhanced time series data (Fig. 8-1).

The conducted experiments demonstrated that our model consistently outperforms existing DL-based super-resolution techniques. This superior performance is evident in a domain adaptation context, specifically when leveraging Sentinel-2 images to generate super-resolution Landsat images. The experimental results not only highlight the efficacy of the proposed model but also emphasize its advantage in scenarios involving different satellite imagery sources. Moreover, the findings confirm that the enhanced multi-temporal RS imagery, achieved through the proposed super-resolution model, contribute substantially to the improvement of fine-grained multi-temporal land use classification. This indicates the practical utility of the developed model in enhancing the quality and precision of land use classification when applied to RS data sets with extended temporal coverage.

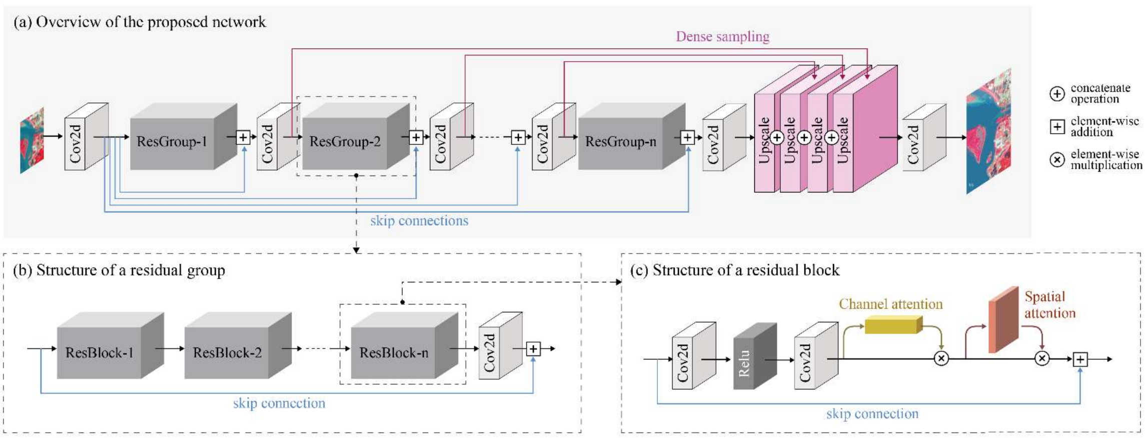

Fig. 8-1. The structure of the proposed method for super-resolution. (a) Overview of the proposed network. (b) Structure of a residual group in the network. (c) Structure of a residual block in a residual group with embedded spatial-channel attention mechanism. We extracted the content of the figure and caption from [67].

8.2 Zhu *et al.*, 2021, IEEE JSTARS: Multi-temporal relearning for land use classification

To derive thematic information from EO-based time series data, we introduce an innovative hybrid classification framework. This framework seamlessly integrates spatial–temporal semantic segmentation with postclassification relearning, specifically designed for multitemporal LULC classification using VHR satellite imagery. The hybrid framework leverages a spatial–temporal semantic segmentation model to capture temporal dependencies and extract high-level spatial–temporal features for accurate classification. Additionally, the principle of postclassification relearning is incorporated to enhance the model's output efficiently. In this process, the initial result from a semantic segmentation model guides a subsequent model through an extended input space, facilitating the end-to-end learning of discriminative feature representations.

Furthermore, OBV is combined with postclassification relearning to address challenges related to high intraclass and low interclass variances (Fig. 8-2). We tested the framework with two postclassification relearning strategies, i.e., pixel-based relearning and object-based relearning, and three CNN models—UNet, a simple Convolutional LSTM, and a UNet Convolutional-LSTM. The experiments were conducted on two data sets featuring LULC labels with rich semantic information and varying urban morphologies, including informal settlements. Each data set encompasses four time steps captured by WorldView-2 and Quickbird imagery. The experimental results unequivocally demonstrate the efficiency of the proposed framework in classifying complex LULC maps using multitemporal VHR images. UNet-ConvLSTM outperforms UNet and the simple ConvLSTM by achieving higher classification accuracy, as well as reflecting temporal consistency in multitemporal LULC classification. It is because a UNet-ConvLSTM takes advantages of encoder–decoder structures, as well as exploits the temporal dependency embedded in the multitemporal data. The most favorable results are obtained with the pixel-based relearning strategy coupled with OBV. Using this model, accuracy of classification maps can exceed 90%. The accuracy levels can be attributed to the complex thematic LULC class categories in this study. Compared with formal settlements, the difference between the building morphologies of informal settlements and rural settlement remains very subtle. Furthermore, the informal settlements in the study area have tiny plot sizes and scatter inside rural settlements. These factors inevitably limited the optimization of classification accuracy. However, these features are not unique to this case study but reflect the reality of many rapidly urbanizing cities around the world which can subsequently be identified and analyzed based on the presented framework.

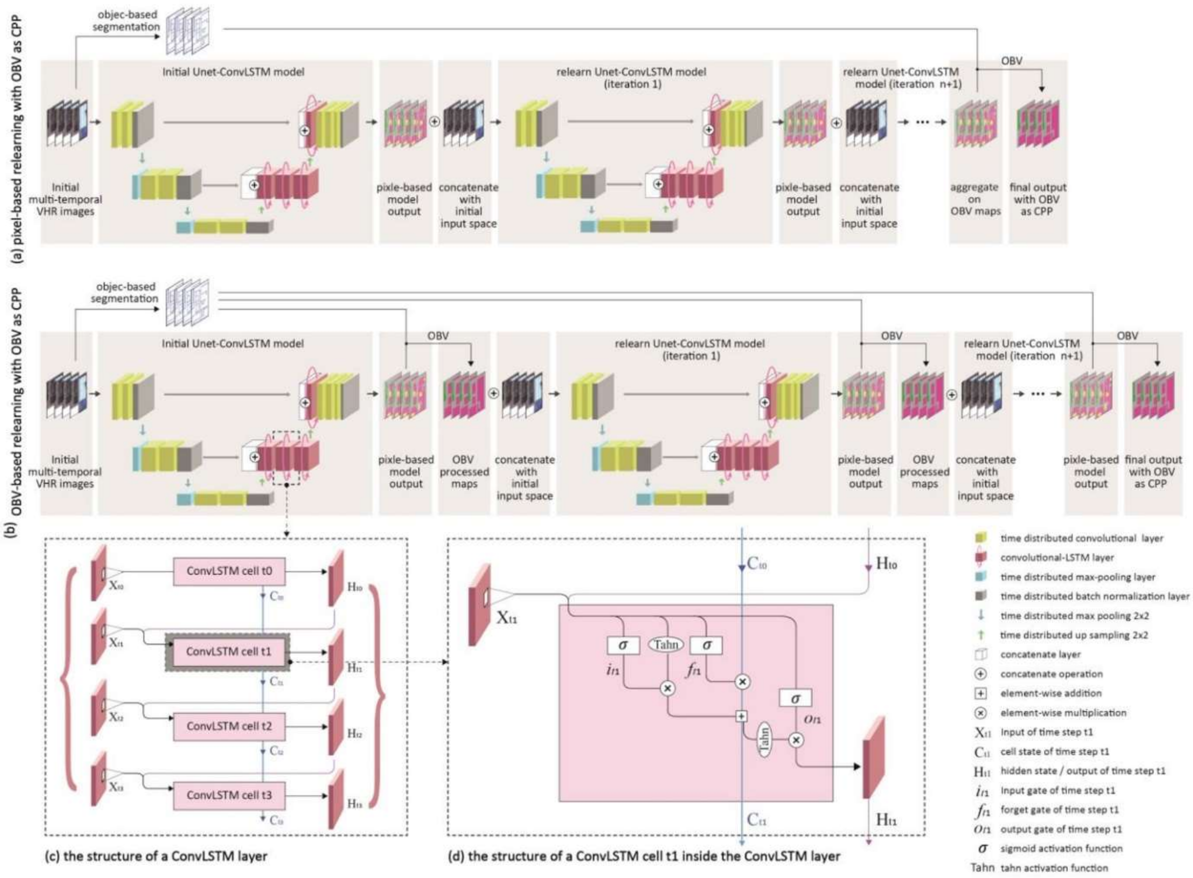

Fig. 8-2. Overview of the two proposed multitemporal relearning frameworks. (a) Pixel-based relearning with OBV as CPP. (b) OBV-based relearning with OBV as CPP. (c) Structure of a ConvLSTM layer. (d) Structure of a ConvLSTM cell inside the ConvLSTM layer. We extracted the content of the figure and caption from [68].

8.3 Zhu *et al.*, 2023, Heliyon: Urban expansion simulation with an explainable ensemble DL

Finally, we developed a DL-based framework for precise geospatial extrapolation of time series data derived from EO sources. This framework is particularly applied in the context of simulating urban expansion, a critical aspect for effective land management and policymaking. We present a novel DL-based ensemble framework designed for urban expansion simulation at an intra-urban granular level. The ensemble framework includes multiple DL models as encoders, transformers for encoding multi-temporal spatial features, convolutional layers for processing single-temporal spatial features, and mechanisms to address the challenge of limited interpretability in DL methods. Notably, the framework incorporates a tailored channel attention block that enables the examination of feature importance, enhancing the interpretability of the model. The proposed method was applied to anticipate urban expansion in Shenzhen, China, showcasing superior performance compared to baseline methods [69], providing also valuable insights for urban planning and decision-making processes.

8.4 Geiß *et al.*, 2023, NHESS: Extrapolation of population in earthquake and tsunami areas

In this study, we extend upon previously developed techniques and utilize EO-based population time series data to project future geospatial population distributions. The focus is on quantifying the prospective number of individuals residing in earthquake-prone and tsunami-prone areas of Lima and Callao, Peru. Leveraging globally existing open-source gridded population time series data sets, we employ ML models tailored for time series analysis—specifically LSTM networks—to predict future time steps. The methodology involves utilizing annual WorldPop population data to project geospatial population distributions over a three-year interval leading up to the year 2035. We implement LSTM and Convolutional LSTM models with both unidirectional and bidirectional learning mechanisms, derived from various feature sets, i.e., driving factors. To gauge the competitive performance of LSTM-based models in this application context, we also implement multilinear regression and RF models for comparison. The results underscore the efficacy of LSTM-based models in forecasting gridded population data. The most accurate prediction is achieved with an LSTM equipped with a bidirectional learning scheme, featuring a root-mean-squared error of 3.63 people per 100 * 100 meters grid cell, while maintaining an excellent model fit. These findings highlight the value of LSTM-based models for precise and reliable projections of future geospatial population distributions.

Model projections are subsequently combined with hazard models for earthquake and tsunami events. Notably, in regions with high peak ground acceleration ranging from 207-210 cm/s^2, the population is expected to grow by almost 30%, constituting 70% of the predicted additional inhabitants for Lima. Additionally, the population in tsunami inundation areas is anticipated to experience a 61% growth until 2035, significantly surpassing the city's average growth rate of 35%. The visual representation of the forecasted population alongside hazard intensities, as depicted in Fig. 8-3 from a south-western viewing angle, reveals new future hot spots of exposed population. These are areas where both high population increases and severe hazard intensities coincide, particularly in Lima and Callao's north-western and south-western settlement areas along the coastline. Anticipating such patterns can be instrumental for urban planners and policymakers in proactively developing effective strategies for risk mitigation. For example, the information about future exposed populations can be integrated into modern decentralized information systems for comprehensive (multi)-risk assessment [71]. This approach allows for informed decision-making and targeted interventions to enhance resilience and reduce vulnerabilities in the face of potential hazards.

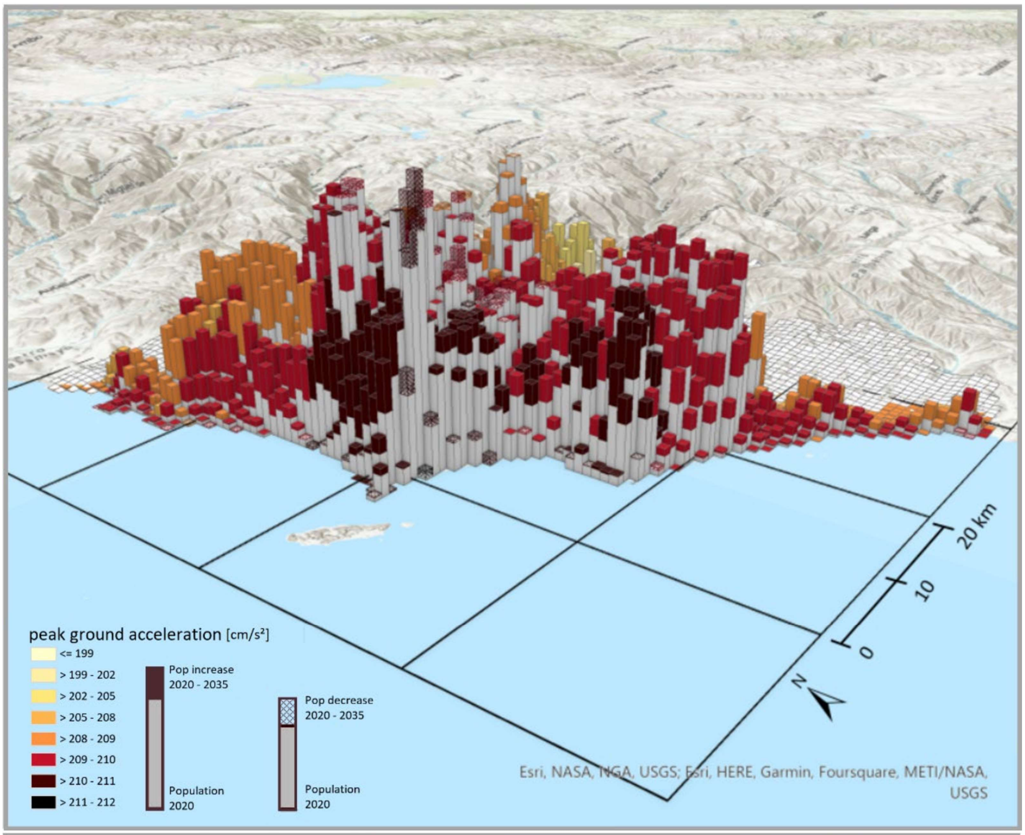

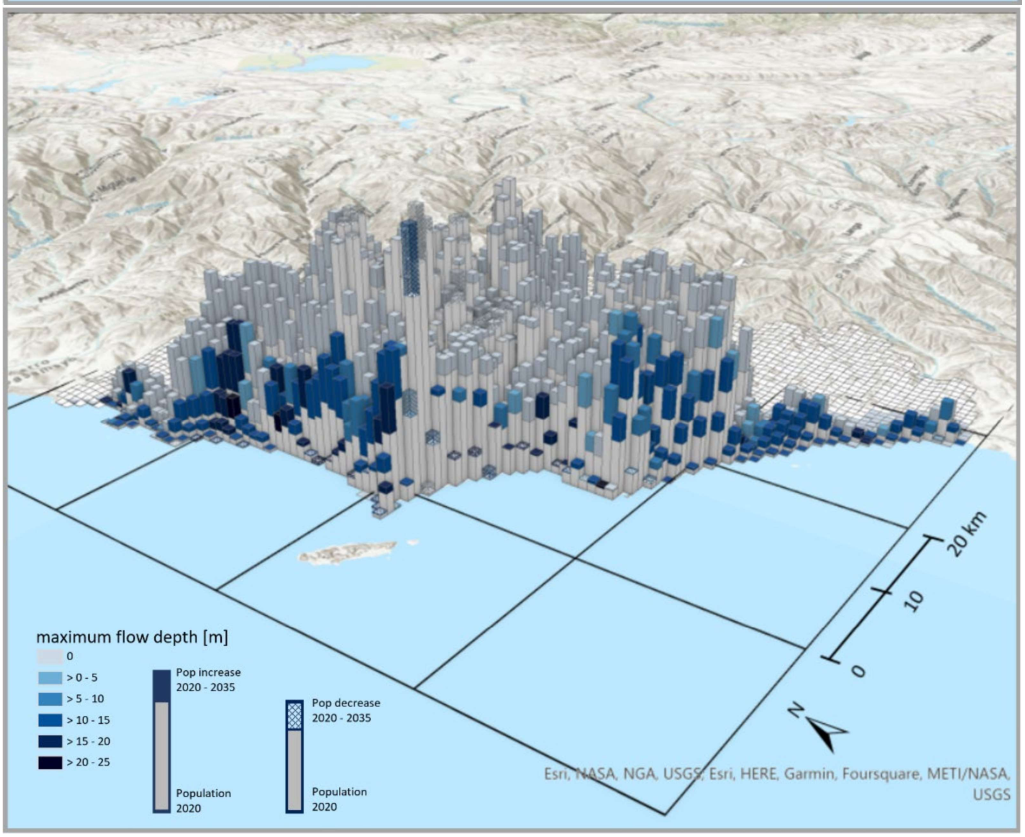

Fig. 8-3. Maps of the predicted population affected by earthquake (top) and tsunami (bottom) for the year 2035 with corresponding hazard intensities. The solid grey bars indicate the population of the year 2020. The additional colored bar (on top) or textured bar indicate the estimated increase or decrease of the population until the year 2035, respectively. The corresponding color coding indicates the hazard intensity. We extracted the content of the figure and caption from [70].

9. Summary and outlook

The new EO missions, the accessibility of RS data archives, the integration of complementary geospatial data sources, as well as the extensive possibilities for a more accurate thematic interpretation of the multimodal geospatial data through advanced ML and AI methods, result in a very broad spectrum of applications in the context of natural hazard risk and impact assessment. It is clear that there has never been a greater abundance of structured multimodal geospatial data pertaining to the built environments on a global scale.

In relation to the objectives outlined above, the exploitation of complementary geospatial data sources comprising EO missions (including Landsat, Sentinel-2, TDM), geospatial vector data compiled by volunteers (i.e., OpenStreetMap), as well as *in-situ* sensing (i.e., street-level imagery) via a collective sensing approach proved useful in the derivation of natural hazard risk-related properties of built environments [46], [49], [50], [51], [53], [60], [67], [69]. From a methodological point of view, advanced concepts and models from the ML/AI domain such as deep (multitask) learning [43], [54], [62], [68], and (semi-supervised) VSVM [27], [32] enabled the accurate thematic interpretation of the geospatial data, while deploying frequently solely a comparably small amount of domain-specific prior knowledge. Also, transfer of models could be successfully addressed via invariant feature selection [63], source-target domain matching [53], and proper source domain selection mechanisms [55], among others. Finally, the considered data and methods were successfully deployed to assess pre-event natural hazard risk w.r.t. earthquakes [56], [60], [63], landslides [64], and multi-risk situations [62], to enable automated post-event damage assessment in the context of earthquakes, tsunamis, and floods [66], and to anticipate future natural hazard-related exposure regarding both earthquakes and tsunamis [70].

Future works can fruitfully address various directions that emerge in the field of deploying RS techniques for natural hazard risk and impact assessment.

- **Refine existing exposure data on large scales**: In this habilitation thesis, we propose an ensemble of data and methods to characterize the built environment in terms of built-up density and built-up height. This ensemble is deployed in a top-down approach for the disaggregation and spatial refinement of existing natural hazard-related exposure data. Empirical results, obtained from a specific metropolitan area, highlight the benefits of the refined data for loss modeling. Consequently, future work can implement the proposed ensemble of methods into a harmonized data processing pipeline to seamlessly characterize built environments on large geographical scales. This approach is particularly valuable for data-scarce regions, allowing for enhanced accuracy in risk assessment procedures. Thereby, it enables the consideration of new and emerging exposure data, such as recent releases from GEM [72], for disaggregation. The techniques mentioned also hold relevance for improving the timely resolution properties of exposure data. This involves estimating variables used for disaggregation across multiple time steps, aiming to evolve from risk assessment procedures, capturing a snapshot in time, to timely continuous monitoring. The latter facilitates frequent risk auditing, providing insights into the effectiveness of risk mitigation measures.

- **Collect exposure data in an automated manner**: From a bottom-up perspective, the proposed techniques that built upon street-level imagery enable the collection of vulnerability-related structural building characteristics with a high degree of automation and accuracy. Subsequent works can extend this approach by integrating it with EO data for a spatially seamless assessment. Furthermore, it is desirable to equip the models with dedicated transfer mechanisms, including the capability to operate under covariate shift: this involves working with street-level imagery from various platforms (e.g., Mapillary). Additionally, the models should automatically adapt to shifted appearances of previously learned classes and detect completely novel classes in a new geographic target domain, i.e., adapt to a potential sample selection bias.
- **Enable natural hazard multi-risk assessment**: Current research focuses on the simultaneous assessment of multiple hazards, recognizing that many regions are prone to various natural hazards. Understanding the interactions and cumulative impacts of multiple hazards is crucial for comprehensive risk assessment. Here, the proposed multitask models, which forecast multiple target variables while considering the interdependencies among them, explicitly aim to tackle multi-risk scenarios from an exposure perspective. Future work can further extent and tailor the list of considered target variables in order to map specific multi-risk situations arising from the sequential unfolding of multiple hazards [73].
- **Compile and share domain-specific training data**: Establishing ML/AI models with high generalization capabilities frequently requires well-curated and annotated data sets used for training. While valuable efforts were made in the context of post-event damage assessment applications [74], the systematic compilation and sharing of annotated data regarding vulnerability-related structural building characteristics remains largely absent. Here, efforts should be carried out to provide well-curated and task-specific data sets to the scientific community for model learning and transfer.

- **Develop general-purpose ML/AI models**: As indicated, procedures for risk and impact assessment often demand domain-specific expertise from various scientific disciplines such as civil engineering, seismology, or hydrology, among others. This expertise is also crucial for compiling and annotating training data utilized in subsequent ML/AI models. Acquiring such domain-specific knowledge is frequently resource-intensive. For instance, our proposed VSVM-based models were explicitly designed to exhibit high generalization capabilities with minimal prior knowledge. In this context, future endeavors could focus on incorporating a representation learning approach, potentially based on techniques that excel in generalizing with limited samples, such as contrastive learning [75]. In parallel, pretraining techniques based on foundation models were recently successfully tailored for EO data interpretation [76]. Prospectively, this presents a promising avenue for minimizing the reliance on extensive domain-specific knowledge, even when confronted with new tasks or modalities [77].
- **Consider comprehensive sets of risk metrics**: The risk assessment metrics applied in this thesis primarily focus on quantifying direct losses concerning building inventories and populations. Subsequent efforts could explore the potential of collective sensing techniques to assess indirect losses and also damage to infrastructure systems and the ramifications of their disruption. Furthermore, involving local communities in the risk assessment process is crucial. This engagement allows for the incorporation of indigenous knowledge, enhancing the understanding of local vulnerabilities and, consequently, improving the effectiveness of downstream risk mitigation strategies.
- **Compute dynamic future scenarios**: In this work, we introduce a collection of techniques designed for geospatial extrapolation of change trajectories in time series data. These methods can serve as the methodological backbone for systematically anticipating future risks, a critical aspect given the frequent changes in built environments over short time frames. In this regard, it is essential to compile time series data related to natural hazard risks, incorporating target variables such as vulnerability-related structural building characteristics and population. Thereby, also interactions with the actual hazard can be assessed, such as the impact of future settlement areas and their properties on microclimates and climate-related natural hazards.

In essence, the objective remains to provide urban planners, civil protection agencies, and policymakers with the necessary data and tools to actively devise successful approaches for minimizing risks. This, in turn, aids in achieving their primary objective: decreasing both the human and economic toll resulting from natural disasters.

References

[1] Munich RE, “Annual statistics,” in: NatCatSERVICE, 2021 [cited Aug. 13th 2021]. Available: http://natcatservice.munichre.com

[2] United Nations Department of Economic and Social Affairs, Population Division, “World Population Prospects 2022: Summary of Results,” UN DESA/POP/2022/TR/NO. 3, 2022.

[3] C. Geiß, E. Schoepfer, T. Riedlinger, and H. Taubenböck, “Editorial: novel tools for multi-risk assessment,” *Nat. Hazards*, vol. 119, pp. 773–778, 2023.

[4] H. Taubenböck, T. Esch, A. Felbier, M. Wiesner, A. Roth, and S. Dech, “Monitoring urbanization in mega cities from space,” *Remote Sens. Environ.*, vol. 117, pp. 162–176, 2012.

[5] United Nations Office for Disaster Risk Reduction, “Global Assessment Report on Disaster Risk Reduction 2022- Our World at Risk: Transforming Governance for a Resilient Future,” Geneva, 2022.

[6] M. Pittore, M. Wieland, and K. Fleming, “Perspectives on global dynamic exposure modelling for geo-risk assessment,” *Nat. Hazards*, vol. 86, pp. 7–30, 2017.

[7] H. Taubenböck, J. Post, A. Roth, K. Zosseder, G. Strunz, and S. Dech, “A conceptual vulnerability and risk framework as outline to identify capabilities of remote sensing,” *Nat. Hazards Earth Syst. Sci.*, vol. 8, pp. 409–420, 2008.

[8] A. Ebert, N. Kerle, and A. Stein, “Urban social vulnerability assessment with physical proxies and spatial metrics derived from air- and spaceborne imagery and GIS data,” *Nat. Hazards*, vol. 48, pp. 275–294, 2009.

[9] C. Aubrecht, D. Özceylan, K. Steinnocher, and S. Freire, “Multi-level geospatial modeling of human exposure patterns and vulnerability indicators,” *Nat. Hazards*, vol. 68, pp. 147–163, 2013.

[10] C. Geiß, H. Taubenböck, S. Tyagunov, A. Tisch, J. Post, and T. Lakes, “Assessment of seismic building vulnerability from space,” *Earthquake Spectra*, vol. 30, no. 4, pp. 1553–1583, 2014.

[11] C. Geiß, P. Aravena Pelizari, M. Marconcini, W. Sengara, M. Edwards, T. Lakes, and H. Taubenböck, “Estimation of seismic buildings structural types using multi-sensor remote sensing and machine learning techniques,” *ISPRS J. Photogramm. Remote Sens.*, vol. 104, pp. 175–188, 2015.

[12] C. Geiß, M. Jilge, T. Lakes, and H. Taubenböck, “Estimation of seismic vulnerability levels of urban structures with multisensor remote sensing,” *IEEE J. Selected Topics Appl. Earth Observ. Remote Sens.*, vol. 9, no. 5, pp. 1913–1936, 2016.

[13] C. Geiß, A. Schauß, T. Riedlinger, S. Dech, C. Zelaya, N. Guzman, M. Hube, J. J. Arsanjani, and H. Taubenböck, “Joint use of remote sensing data and volunteered geographic information for exposure estimation – evidence from Valparaíso, Chile,” *Nat. Hazards*, vol. 86, pp. 81–105, 2017.

[14] C. Geiß, and H. Taubenböck, “One step back for a leap forward: toward operational measurements of elements at risk,” *Nat. Hazards*, vol. 86, pp. 1–6, 2017.

[15] M. Drusch, U. Del Bello, S. Carlier, O. Colin, V. Fernandez, F. Gascon, B. Hoersch, C. Isola, P. Laberinti, P. Martimort, A. Meygret, F. Spoto, O. Sy, F. Marchese, and P. Bargellini “Sentinel-2: ESA’s optical high-resolution mission for GMES operational services,” *Remote Sens. Environ.*, vol. 120, pp. 25–36, 2012.

[16] G. Krieger, A. Moreira, H. Fiedler, I. Hajnsek, M. Werner, M. Younis, and M. Zink “TanDEM-X: A satellite formation for high-resolution SAR interferometry,” *IEEE Trans. Geosci. Remote Sens.*, vol. 45, no. 11, pp. 3317–3341, 2007.

[17] M. Zink, M. Bachmann, B. Bräutigam, T. Fritz, I. Hajnsek, G. Krieger, A. Moreira, and B. Wessel “TanDEM-X: The new global DEM takes shape,” *IEEE Geosci. Remote Sens. Mag.*, vol. 2, no. 2, pp. 8–23, Jun. 2014.

[18] B. Herfort, S. Lautenbach, J. Porto de Albuquerque, J. Anderson, and A. Zipf, “A spatio-temporal analysis investigating completeness and inequalities of global urban building data in OpenStreetMap,” *Nat Commun.*, vol. 14, 3985, 2023.

[19] M. Wieland, M. Pittore, S. Parolai, J. Zschau, B. Moldobekov, and U. Begaliev, “Estimating building inventory for rapid seismic vulnerability assessment: Towards an integrated approach based on multisource imaging,” *Soil Dyn. Earthquake Eng.*, vol. 36, pp. 70–83, 2012.

[20] D. Anguelov, C. Dulong, D. Filip, C. Frueh, S. Lafon, R. Lyon, A. Ogale, L. Vincent, and J. Weaver “Google street view: Capturing the world at street level,” *Computer*, vol. 43, no. 6, pp. 32–38, Jun. 2010.

[21] H. Taubenböck, J. Staab, X. Zhu, C. Geiß, S. Dech, and M. Wurm, “Are the poor digitally left behind? Indications of urban divides based on remote sensing and twitter data,” *ISPRS Int. J. Geo-Inf.*, vol. 7, no. 8, 2018.

[22] Y. LeCun, Y. Bengio, and G. Hinton, “Deep learning,” *Nature*, vol. 521, pp. 436–444, 2015.

[23] G. Camps-Valls, and L. Bruzzone, “Kernel Methods for Remote Sensing Data Analysis,” John Wiley & Sons, New York, 2009.

[24] C. Geiß, M. Klotz, A. Schmitt, and H. Taubenböck, “Object-based Morphological Profiles for Classification of Remote Sensing Imagery,” *IEEE Trans. Geosci. Remote Sens.*, vol. 54, no. 10, pp. 5952–5963, 2016.

[25] G. Camps-Valls, D. Tuia, L. Bruzzone, and J. A. Benediktsson, “Advances in Hyperspectral Image Classification: earth monitoring with statistical learning methods,” *IEEE Signal Process. Mag.*, vol. 31, no. 1, pp. 45–54, 2014.

[26] E. Izquierdo-Verdiguier, V. Laparra, L. Gómez-Chova, and G. Camps-Valls, “Encoding invariances in remote sensing image classification with SVM,” *IEEE Geosci. Remote Sens. Lett.*, vol. 10, no. 5, pp. 981–985, 2013.

[27] C. Geiß, P. Aravena Pelizari, L. Blickensdörfer, and H. Taubenböck, “Virtual Support Vector Machines with Self-Learning Strategy for Classification of Multispectral Remote Sensing Imagery,” *ISPRS J. Photogramm. Remote Sens.*, vol. 151, pp. 42–58, 2019.

[28] Y.-F. Li, and Z.-H. Zhou, “Towards Making Unlabeled Data Never Hurt,” *IEEE Trans. Pattern Anal. Mach. Intell.*, vol. 37, no. 1, pp. 175–188, 2015.

[29] C. Geiß, M. Thoma, M. Pittore, M., Wieland, S. Dech, and H. Taubenböck, “Multitask Active Learning for Characterization of Built Environments with Multisensor Earth Observation Data,” *IEEE J. Selected Topics Appl. Earth Observ. Remote Sens.*, vol. 10, no. 12, pp. 5583–5597, 2017.

[30] C. Geiß, M. Thoma, and H. Taubenböck, “Cost-sensitive Multitask Active Learning for Characterization of Urban Environments with Remote Sensing,” *IEEE Geosci. Remote Sens. Lett.*, vol. 15, no. 6, pp. 922–926, 2018.

[31] C. Persello, and L. Bruzzone, “Active and Semisupervised Learning for the Classification of Remote Sensing Images,” *IEEE Trans. Geosci. Remote Sens.*, vol. 52, no. 11, pp. 6937–6956, 2014.

[32] C. Geiß, P. Aravena Pelizari, O. Tuncbilek, and H. Taubenböck, “Semi-supervised Learning with Constrained Virtual Support Vector Machines for Classification of Remote Sensing Image Data,” *Int. J. Appl. Earth Obs. Geoinf.*, vol. 125, 103571, 2023.

[33] L. Bruzzone, and L. Carlin, “A multilevel context-based system for classification of very high spatial resolution images,” *IEEE Trans. Geosci. Remote Sens.*, vol. 44, no. 9, pp. 2587–2600, 2006.

[34] J. Li, X. Huang, and J. Gong, “Deep neural network for remote-sensing image interpretation: Status and perspectives,” *Nat. Sci. Rev.*, vol. 6, no. 6, pp. 1082–1086, 2019.

[35] J. Long, E. Shelhamer, and T. Darrell, “Fully Convolutional Networks for Semantic Segmentation,” in *Proc. IEEE Conf. Comput. Vision Pattern Recog.*, 2015.

[36] X. Huang, Q. Lu, L. Zhang, and A. Plaza, “New postprocessing methods for remote sensing image classification: A systematic study,” *IEEE Trans. Geosci. Remote Sens.*, vol. 52, no. 11, pp. 7140–7159, 2014.

[37] J. Stuckens, P. R. Coppin, and M. E. Bauer, “Integrating contextual information with per-pixel classification for improved land cover classification,” *Remote Sens. Environ.*, vol. 71, no. 3, pp. 282–296, 2000.

[38] C. Geiß and H. Taubenböck, “Object-based postclassification relearning,” *IEEE Geosci. Remote Sens. Lett.*, vol. 12, no. 11, pp. 2336–2340, 2015.

[39] X. Han, X. Huang, J. Li, Y. Li, M. Y. Yang, and J. Gong, “The edgepreservation multi-classifier relearning framework for the classification of high-resolution remotely sensed imagery,” *ISPRS J. Photogramm. Remote Sens.*, vol. 138, pp. 57–73, 2018.

[40] Q. Shi, X. Liu, and X. Huang, “Active relearning framework for remote sensing image classification,” *IEEE Trans. Geosci. Remote Sens.*, vol. 56, no. 6, pp. 3468–3485, 2018.

[41] D. H. Wolpert, “Stacked generalization,” *Neural Netw.*, vol. 5, no. 2, pp. 241–259, 1992.

[42] D. Marmanis, K. Schindler, J. D. Wegner, S. Galliani, M. Datcu, and U. Stilla, “Classification with an edge: Improving semantic image segmentation with boundary detection,” *ISPRS J. Photogramm. Remote Sens.*, vol. 135, pp. 158–172, 2018.

[43] C. Geiß, Y. Zhu, C. Qiu, L. Mou, X. X. Zhu, and H. Taubenböck, “Deep Relearning in the Geospatial Domain for Semantic Remote Sensing Image Segmentation,” *IEEE Geosci. Remote Sens. Lett.*, vol. 19, 8002705, 2022.

[44] T. Esch, W. Heldens, A. Hirner, M. Keil, M. Marconcini, A. Roth, J. Zeidler, S. Dech, and E. Strano, “Breaking new ground in mapping human settlements from space–The Global Urban Footprint,” *ISPRS J. Photogramm. Remote Sens.*, vol. 134, pp. 30–42, 2017.

[45] C. Corbane, M. Pesaresi, P. Politis, V. Syrris, A. J. Florczyk, P. Soille, L. Maffenini, A. Burger, V. Vasilev, D. Rodriguez, D., F. Sabo, L. Dijkstra, and T. Kemper, “Big earth data analytics on Sentinel-1 and Landsat imagery in support to global human settlements mapping,” *Big Earth Data*, vol. 1, pp. 118–144, 2017.

[46] C. Qiu, M. Schmitt, C. Geiß, T-H. K. Chen, and X. X. Zhu, “A framework for large-scale mapping of human settlement extent from Sentinel-2 images via fully convolutional networks,” *ISPRS J. Photogramm. Remote Sens.*, vol. 163, pp. 152–170, 2020.

[47] O. Ronneberger, P. Fischer, and T. Brox, “U-Net: Convolutional networks for biomedical image segmentation,” in *Proc. Int. Conf. Med. Image Comput. Comput.-Assist. Interv.*, pp. 234–241, 2015.

[48] W. Yao, Z. Zeng, C. Lian, and H. Tang, “Pixel-wise regression using U-Net and its application on pansharpening,” *Neurocomputing*, vol. 312, pp. 364–371, 2018.

[49] K. Müller, R. Leppich, C. Geiß, V. Borst, P. Aravena Pelizari, S. Kounev, and H. Taubenböck, “Deep Neural Network Regression for Digital Surface Model Generation with Sentinel-2 Imagery,” *IEEE J. Selected Topics Appl. Earth Observ. Remote Sens.*, vol. 16, pp. 8508–8519, 2023.

[50] C. Geiß, P. Aravena Pelizari, S. Bauer, A. Schmitt, and H. Taubenböck, “Automatic Training Set Compilation with Multisource Geodata for DTM Generation from the TanDEM-X DSM,” *IEEE Geosci. Remote Sens. Lett.*, vol. 17, no. 3, pp. 456–460, 2022.

[51] C. Geiß, T. Leichtle, M. Wurm, P. Aravena Pelizari, I. Standfuß, X. X. Zhu, E. So, S. Siedentop, T. Esch, and H. Taubenböck, “Large-Area Characterization of Urban Morphology – Mapping Built-Up Height and Density with the TanDEM-X Mission and Sentinel-2,” *IEEE J. Selected Topics Appl. Earth Observ. Remote Sens.*, vol. 12, no. 8, pp. 2912–2927, 2019.

[52] B. Wessel, M. Huber, C. Wohlfart, U. Marschalk, D. Kosmann, and A. Roth, “Accuracy assessment of the global TanDEM-X digital elevation model with GPS data,” *ISPRS J. Photogramm. Remote Sens.*, vol. 139, pp. 171–182, 2018.

[53] C. Geiß, H. Schrade, P. Aravena Pelizari, and H. Taubenböck, “Multistrategy Ensemble Regression for Mapping of Built-Up Height and Density with Sentinel-2 Data,” *ISPRS J. Photogramm. Remote Sens.*, vol. 170, pp. 57–71, 2020.

[54] C. Geiß, E. Brzoska, P. Aravena Pelizari, S. Lautenbach, and H. Taubenböck, “Multi-target Regressor Chains with Repetitive Permutation Scheme for Characterization of Built Environments with Remote Sensing,” *Int. J. Appl. Earth Obs. Geoinf.*, vol. 106, 102657, 2022.

[55] C. Geiß, A. Rabuske, P. Aravena Pelizari, S. Bauer, and H. Taubenböck, “Selection of Unlabeled Source Domains for Domain Adaptation in Remote Sensing,” *Array*, vol. 15, 100233, 2022.

[56] C. Geiß, P. Priesmeier, P. Aravena Pelizari, A. Soto, E. Schöpfer, T. Riedlinger, M. Villar Vega, H. Santa Maria, C. Gomez Zapata, M. Pittore, E. So, A. Fekete, and H. Taubenböck, “Benefits of Global Earth Observation Missions for Disaggregation of Exposure Data and Earthquake Loss Modelling – Evidence from Santiago de Chile,” *Nat. Haz.*, vol. 119, pp. 779–804, 2023.

[57] M. Pittore, M., Haas, and K. G. Megalooikonomou, “Risk-oriented, bottom-up modelling of building portfolios with faceted taxonomies,” *Front. Built Environ.*, vol. 4, 2018.

[58] S. Brzev, C. Scawthorn, A. W. Charleson, L. Allen, M. Greene, K. Jaiswal, and V. Silva, “GEM Building Taxonomy Version 2.0,” *GEM Technical Report 2013-02 V1.0.0.*, GEM Foundation, Pavia, Italy, 2013.

[59] V. Silva, C. Yepes-Estrada, J. Dabbeek, L. Martins, and S. Brzev, “GED4ALL – Global Exposure Database for Multi-Hazard Risk Analysis – Multi-Hazard Exposure Taxonomy,” *GEM Technical Report 2018-01*, GEM Foundation, Pavia, Italy, 2018.

[60] P. Aravena Pelizari, C. Geiß, P. Aguirre, H. Santa María, Y. Merino Peña, and H. Taubenböck, “Automated building characterization for seismic risk assessment using street-level imagery and deep learning,” *ISPRS J. Photogramm. Remote Sens.*, vol. 180, pp. 370–386, 2021.

[61] V. Silva, S. Brzev, C. Scawthorn, C. Yepes, J. Dabbeek, and H. Crowley, “A building classification system for multi-hazard risk assessment,” *Int. J. Disaster risk Sci.*, vol. 13, pp. 161–177, 2022.

[62] P. Aravena Pelizari, C. Geiß, S. Groth, and H. Taubenböck, “Deep multitask learning with label interdependency distillation for multicriteria street-level image classification,” *ISPRS J. Photogramm. Remote Sens.*, vol. 204, pp. 275–290, 2023.

[63] M. Liuzzi, P. Aravena Pelizari, C. Geiß, A. Masi, V. Tramutoli, and H. Taubenböck, “A Transferable Remote Sensing Approach to Classify Building Structural Types for Seismic Risk Analyses: the case of Val d’Agri Area (Italy),” *Bull. Earthq. Eng.*, vol. 17, pp. 4825–4853, 2019.

[64] M. Kühnl, M. Sapena, M. Wurm, C. Geiß, and H. Taubenböck, “Multitemporal Landslide Exposure and Vulnerability Assessment in Medellín, Colombia,” *Nat. Haz.*, vol. 119, pp. 883–906, 2022.

[65] C. Geiß, and H. Taubenböck, “Remote sensing contributing to assess earthquake risk: from a literature review towards a roadmap,” *Nat. Haz.*, vol. 68, pp. 7–48, 2013.

[66] L. Moya, C. Geiß, M. Hashimoto, E. Mas, S. Koshimura, and G. Strunz, “Hazard Intensity-Based Selection of Training Samples for Remote Sensing Building Damage Classification,” *IEEE Trans. Geosci. Remote Sens.*, vol. 59, no. 10, pp. 8288–8304, 2021.

[67] Y. Zhu, C. Geiß, and E. So, “Image Super-Resolution with Dense-sampling Residual Channel-Spatial Attention Networks for Multi-temporal Remote Sensing Image Classification,” *Int. J. Appl. Earth Obs. Geoinf.*, vol. 104, 102543, 2021.

[68] Y. Zhu, C. Geiß, E. So, and Y. Jin, “Multi-temporal Relearning with Convolutional LSTM Models for Land Use Classification,” *IEEE J. Selected Topics Appl. Earth Observ. Remote Sens.*, vol. 14, pp. 3251–3265, 2021.

[69] Y. Zhu, C. Geiß, E. So., R. Bardhan, H. Taubenböck, and Y. Jin, “Urban expansion simulation with an explainable ensemble deep learning framework,” *Heliyon*, forthcoming, 2023.

[70] C. Geiß, J. Maier, E. So, E. Schoepfer, S. Harig, J. C. Gómez Zapata, and Y. Zhu, “Anticipating a risky future: LSTM models for spatiotemporal extrapolation of population data in areas prone to earthquakes and tsunamis in Lima, Peru,” *Nat. Hazards Earth Syst. Sci.*, forthcoming, 2023.

[71] E. Schoepfer, J. Lauterjung, T. Riedlinger, H. Spahn, J. C. Gómez Zapata, C. D. León, H. Rosero-Velásquez, S. Harig, M. Langbein, N. Brinckmann, G. Strunz, C. Geiß, and H. Taubenböck, “Between global risk reduction goals, scientific-technical capabilities and local realities: a novel modular approach for multi-risk assessment,” *Nat. Hazards Earth Syst. Sci.*, forthcoming, 2023.

[72] C. Yepes-Estrada, A. Calderon, C. Costa, H. Crowley, J. Dabbeek, M. Hoyos, L. Martins, N. Paul, A. Rao, and V. Silva, “Global Building Exposure Model for Earthquake Risk Assessment,” *Earthquake Spectra*, vol. 39, no. 4, pp. 2212–2235, 2023.

[73] J. C. Gill and B. D. Malamud, “Hazard interaction networks (cascades) within multi-hazard methodologies,” *Earth Syst. Dynam.*, vol. 7, pp. 659–679, 2016.

[74] R. Gupta, B. Goodman, N. Patel, R. Hosfelt, S. Sajeev, E. Heim, J. Doshi, K. Lucas, H. Choset, and M. Gaston, “Creating xBD: A dataset for assessing building damage from satellite imagery,” *Proceedings of the IEEE/CVF conference on computer vision and pattern recognition workshops*, pp. 10–17, 2019.

[75] A. Jaiswal, A. Ramesh Babu, M. Zaki Zadeh, D. Banerjee, and F. Makedon, “A Survey on Contrastive Self-Supervised Learning,” *Technologies*, vol. 9, no. 2, 2021.

[76] D. Hong, B. Zhang, X. Li, Y. Li, C. Li, J. Yao, N. Yokoya, H. Li, P. Ghamisi, X. Jia, A. Plaza, P. Gamba, J. A. Benediktsson, and J. Chanussot, “SpectralGPT: Spectral foundation model,” arXiv preprint arXiv:2311.07113, 2023.

[77] N. Rahaman, M. Weiss, F. Träuble, F. Locatello, A. Lacoste, Y. Bengio, C. Pal, L. E. Li, and B. Schölkopf, “A General Purpose Neural Architecture for Geospatial Systems,” *AI + HADR Workshop at 36th Conference on Neural Information Processing Systems* (NeurIPS 2022), 2022.